NASA Tech Briefs

National Aeronautics and Space Administration

Electronic Components and Circuits

Electronic Systems

Physical Sciences

Materials

Computer Programs

Mechanics

Machinery

Fabrication Technology

Mathematics and Information Sciences

Life Sciences

99-03

March 1999

INTRODUCTION

Tech Briefs are short announcements of new technology derived from the research and development activities of the National Aeronautics and Space Administration. These Briefs emphasize information considered likely to be transferable across industrial, regional, or disciplinary lines and are issued to encourage commercial application.

Availability of NASA Tech Briefs and TSP's

Distribution of NASA Tech Briefs, a monthly periodical publication, is limited to engineers in U.S. Industry and to other domestic technology transfer agents. Requests for individual Tech Briefs or for Technical Support Packages (TSP's) announced herein should be addressed to

NASA Center for AeroSpace Information
Technology Transfer Office
800 Elkridge Landing Rd.
Linthicum Heights, MD 21090-2934
Telephone No. (301) 621-0245

Please reference the three-letter, five-digit control number located at the end of each Tech Brief. Information on NASA's Technology Utilization Program, its documents, and services is also available at the same facility.

Technology Utilization Officers and Patent Counsels are located at NASA field installations to provide technology-transfer access to industrial users. Inquiries can be made by writing to NASA field installations listed below.

Technology Utilization Officers and Patent Counsels

Ames Research Center
Technology Utilization Officer
Mail Code 223-3
Moffett Field, CA 94035

Patent Counsel
Mail Code 200-11
Moffett Field, CA 94035

Goddard Space Flight Center
Technology Utilization Officer
Mail Code 702-1
Greenbelt, MD 20771

Patent Counsel
Mail Code 204
Greenbelt, MD 20771

Lyndon B. Johnson Space Center
Technology Utilization Officer
Mail Code IC-4
Houston, TX 77058

Patent Counsel
Mail Code AL3
Houston, TX 77058

John F. Kennedy Space Center
Technology Utilization Officer
Mail Stop PT-PMO-A
Kennedy Space Center, FL 32899

Patent Counsel
Mail Code PT-PAT
Kennedy Space Center, FL 32899

Langley Research Center
Technology Utilization Officer
Mail Stop 143
Hampton, VA 23665

Patent Counsel
Mail Code 279
Hampton, VA 23665

Lewis Research Center
Technology Utilization Officer
Mail Stop 7-3
21000 Brookpark Road
Cleveland, OH 44135

Patent Counsel
Mail Code LE-LAW
21000 Brookpark Road
Cleveland, OH 44135

Jet Propulsion Laboratory
Technology Utilization Officer
Mail Stop 156-211
4800 Oak Grove Drive
Pasadena, CA 91109

NASA Resident Office-JPL
Technology Utilization Officer
Mail Stop 180-801
4800 Oak Grove Drive
Pasadena, CA 91109

Patent Counsel
Mail Code 180-801
4800 Oak Grove Drive
Pasadena, CA 91109

George C. Marshall Space Flight Center
Technology Utilization Officer
Code AT01
Marshall Space Flight Center, AL 35812

Patent Counsel
Mail Code CC01
Marshall Space Flight Center, AL 35812

John C. Stennis Space Center
Technology Utilization Officer
Code HA-30
Stennis Space Center, MS 39529

NASA Headquarters
Technology Utilization Officer
Code CU
Washington, DC 20546

Assistant General Counsel for Patent Matters
Code GP
Washington, DC 20546

Dryden Flight Research Center
Technology Utilization Officer
M/S D21-31
Bldg. 4832 Whse 7
Lilly Dr.
Edwards, CA 93523

BLANK PAGE

NASA TechBriefs

National Aeronautics and Space Administration

March 1999
99-03

BLANK PAGE

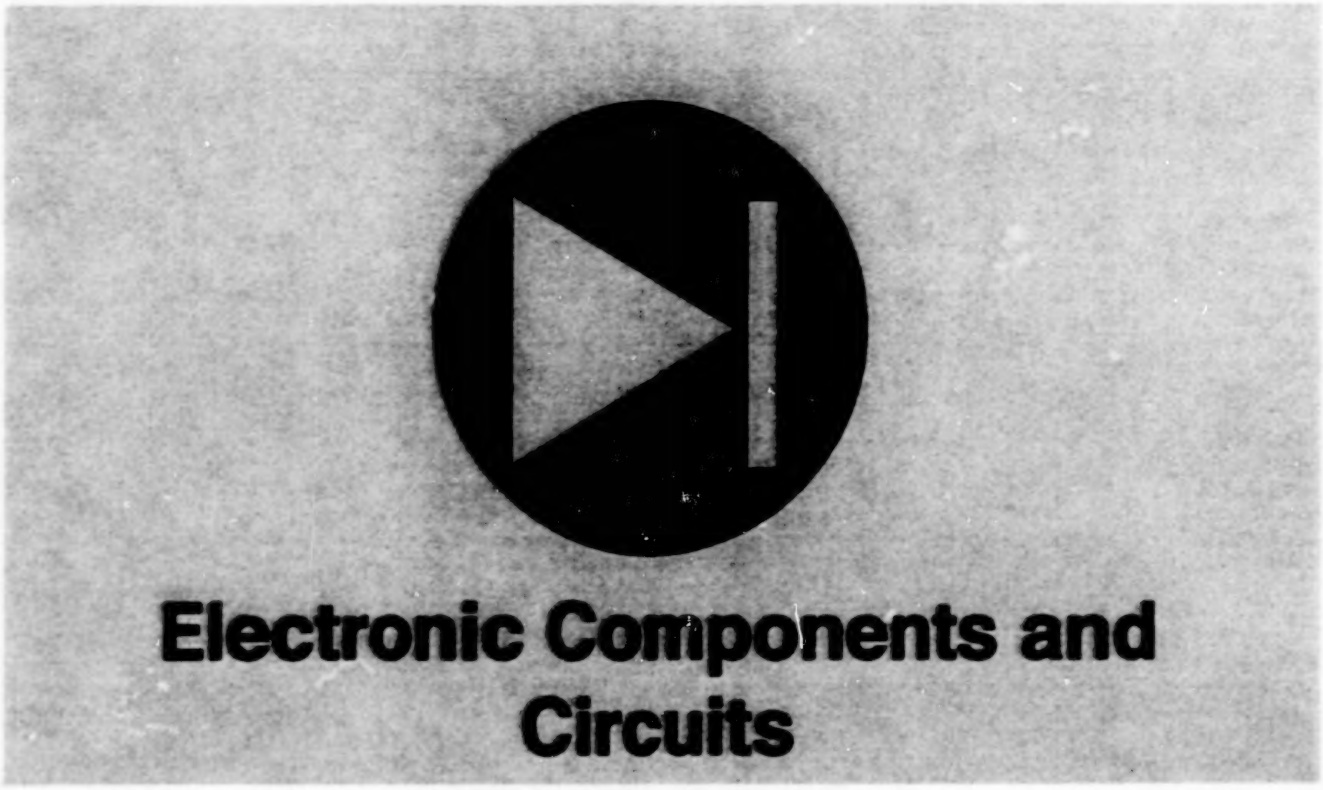

Electronic Components and Circuits

Hardware, Techniques, and Processes

BLANK PAGE

Interdigital Overlay Capacitors for Integrated Circuits

A given amount of capacitance can be accommodated on less chip area.

NASA's Jet Propulsion Laboratory, Pasadena, California

Interdigital overlay capacitors have been invented to decrease the amount of integrated-circuit chip area needed to accommodate a given amount of capacitance. In most very-large-scale integrated (VLSI) circuits and monolithic microwave integrated circuits (MMIC), the integrated capacitors are the largest circuit elements. By making it possible to fit the capacitors within smaller chip areas, this invention offers the potential to reduce the overall chip sizes, increase the numbers of circuit elements that can be accommodated on given chip areas, and/or satisfy increasingly stringent design constraints on the dimensions of circuit elements.

An interdigital overlay capacitor is a multilayer parallel-plate capacitor with thin layers of dielectric material between the electrodes. It is so named because its electrodes appear interdigitated in a cross-sectional view (see Figure 1) and because its layers are stacked or overlaid on an integrated-circuit chip. The chip area occupied by an interdigital overlay capacitor is the same as that of a conventional dielectric-overlay capacitor, which contains only one dielectric layer and thus has less capacitance.

Prototype interdigitated overlay capacitors have been made by use of established integrated-circuit fabrication techniques: The metal electrode layers were made by evaporative deposition of Ti sublayers to a thickness of 300 Å and Au sublayers to a thickness of 2,000 Å. The dielectric layers were made by deposition of a nitride material deposited from a room-temperature electron-cyclotron-resonance plasma, with patterning by a lift-off photolithographic process. The relative permittivity of the dielectric layers was ≈6, and the thickness of each dielectric layer was about 1,200 Å. To provide a taper needed to ensure a high yield of the fabrication process, each metal layer in a stack was recessed from the one below it by a margin of 5 μm.

Figure 2 is a plot of measured capacitances of prototype one-, two-, and three-layer interdigitated overlay capacitors versus overlapping electrode area. These measurements show that the capacitance was doubled from 9 pF (for one layer) to 18 pF (for three layers) without increasing the capacitor base area.

This work was done by Trong-Huang Lee, Jeff Hong, and Imran Mehdi of Caltech for **NASA's Jet Propulsion Laboratory.**

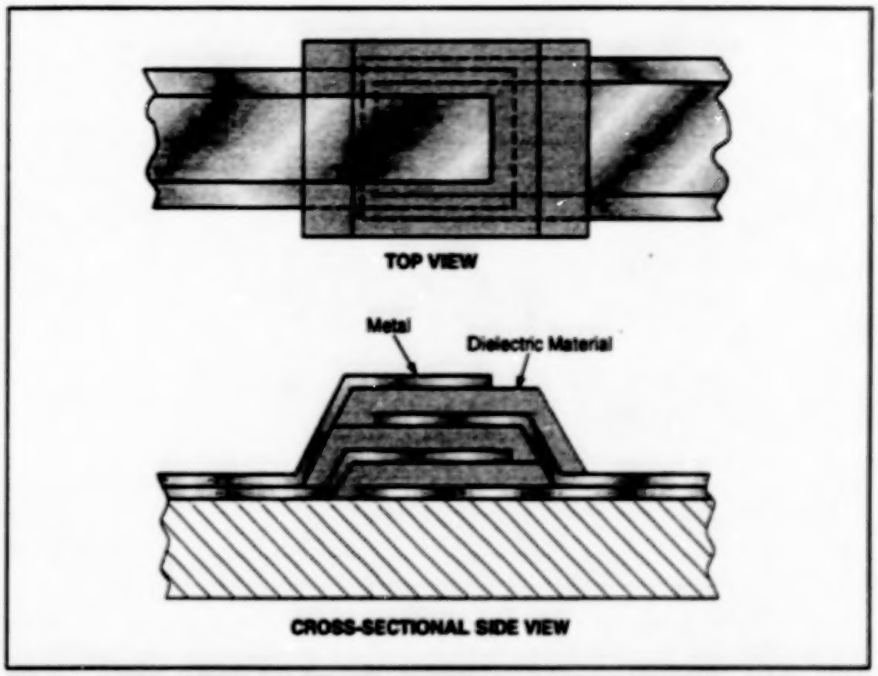

Figure 1. Layers of Metal and Dielectric Material are stacked in alternation, and the metal electrodes are connected alternately to two terminals to form a multilayer capacitor.

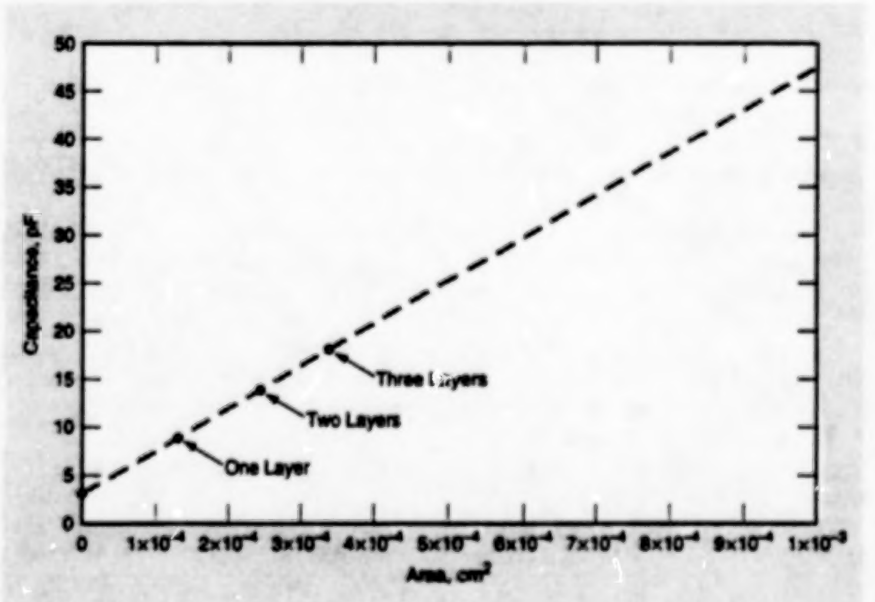

Figure 2. Measurements of Capacitance (*C*) vs. Overlapping Electrode Area (*A*) have been fitted with a straight line represented by the equation $C = 4.4 \times 10^4 A + 3.35$. The 3.35 pF is a fringing capacitance.

Further information is contained in a TSP [see page 1].

In accordance with Public Law 96-517, the contractor has elected to retain title to this invention. Inquiries concerning rights for its commercial use should be addressed to

Technology Reporting Office
JPL
Mail Stop 122-116
4800 Oak Grove Drive
Pasadena, CA 91109
(818) 354-2240

Refer to NPO-20383, volume and number of this NASA Tech Briefs *issue, and the page number.*

Microwave Heating With Uniform Temperature History

All parts of a process stream or a stationary sample are processed equally.

NASA's Jet Propulsion Laboratory, Pasadena, California

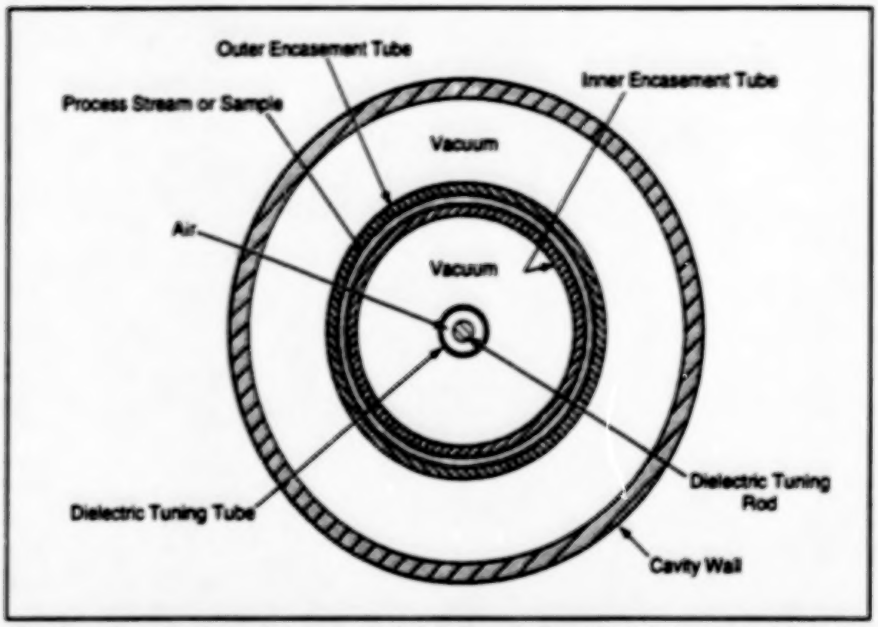

The Sample or Process Stream Is Heated Uniformly throughout its interior because it is confined in a narrow annular region that contains an antinode of an axisymmetric TM_{010} electromagnetic mode of the microwave cavity, which has no axial dependence.

Several microwave-cavity devices at various stages of development are designed for heating material samples or process streams with uniform temperature-versus-time histories. These devices could satisfy needs for heating according to well-regulated temperature-vs.-time schedules for batch and stream processing in diverse applications; for example, pharmaceutical processing, extrusion and molding of plastics, and processing of biological or medical samples.

The figure presents a simplified axial cross-sectional view of one such device for heating either (1) a stationary annular or cylindrical sample of material or (2) a process stream flowing axially, with azimuthal uniformity, in a narrow space between an inner and an outer encasement tube. The geometry of the device is chosen so that in the plane of the figure or any other plane along the cylindrical axis, the process stream or sample is exposed to substantially equal microwave power density at all points along its circumference.

The microwave cavity is dimensioned to support an axisymmetric mode, and the radii of the inner and outer encasement tubes are chosen so that the annular sample or flow space between these tubes contains an antinode of either the electric or the magnetic field. This choice of dimensions minimizes the spatial variation of the electric or magnetic field within the sample, thereby minimizing spatial variations in the heating rate. The encasement tubes should be made of a low-loss dielectric material; for example, quartz.

If the sample or process stream is of a lossy dielectric material (e.g., a plastic), then for maximum and substantially uniform heating, the annular space should be dimensioned to contain an antinode of the electric field. Similarly, if the material in question is subject to heating predominantly by the magnetic field, then the annulus should be dimensioned to contain an antinode of the magnetic field.

To prevent convective cooling of the heated sample or process stream, the empty spaces within the microwave cavity are evacuated. To minimize radiative cooling, the cavity wall and end plates are coated with gold, which is highly reflective of thermal radiation. The innermost part of the cavity is occupied by a fixed dielectric tube and an axially movable dielectric rod within the tube; these components are used to tune the cavity to resonance at the frequency of a magnetron or other source that supplies the microwave power. [Tuning by use of this technique was described in "Improved Tuning of a Microwave Cavity for Heating Samples" (NPO-20409), *NASA Tech Briefs*, Vol. 22, No. 11 (November 1998), page 54.] In the case of a process flow, the tuning rod and tube can be tapered to compensate for the variation of the permittivity of the material with temperature and thus with axial position, to keep the desired field antinode within the annulus at all axial positions.

This work was done by Henry W. Jackson of Acro Service Corp. and Martin Barmatz of Caltech for **NASA's Jet Propulsion Laboratory**. *Further information is contained in a TSP [see page 1].*

In accordance with Public Law 96-517, the contractor has elected to retain title to this invention. Inquiries concerning rights for its commercial use should be addressed to

Technology Reporting Office
JPL
Mail Stop 122-116
4800 Oak Grove Drive
Pasadena, CA 91109
(818) 354-2240

Refer to NPO-20459, volume and number of this NASA Tech Briefs *issue, and the page number.*

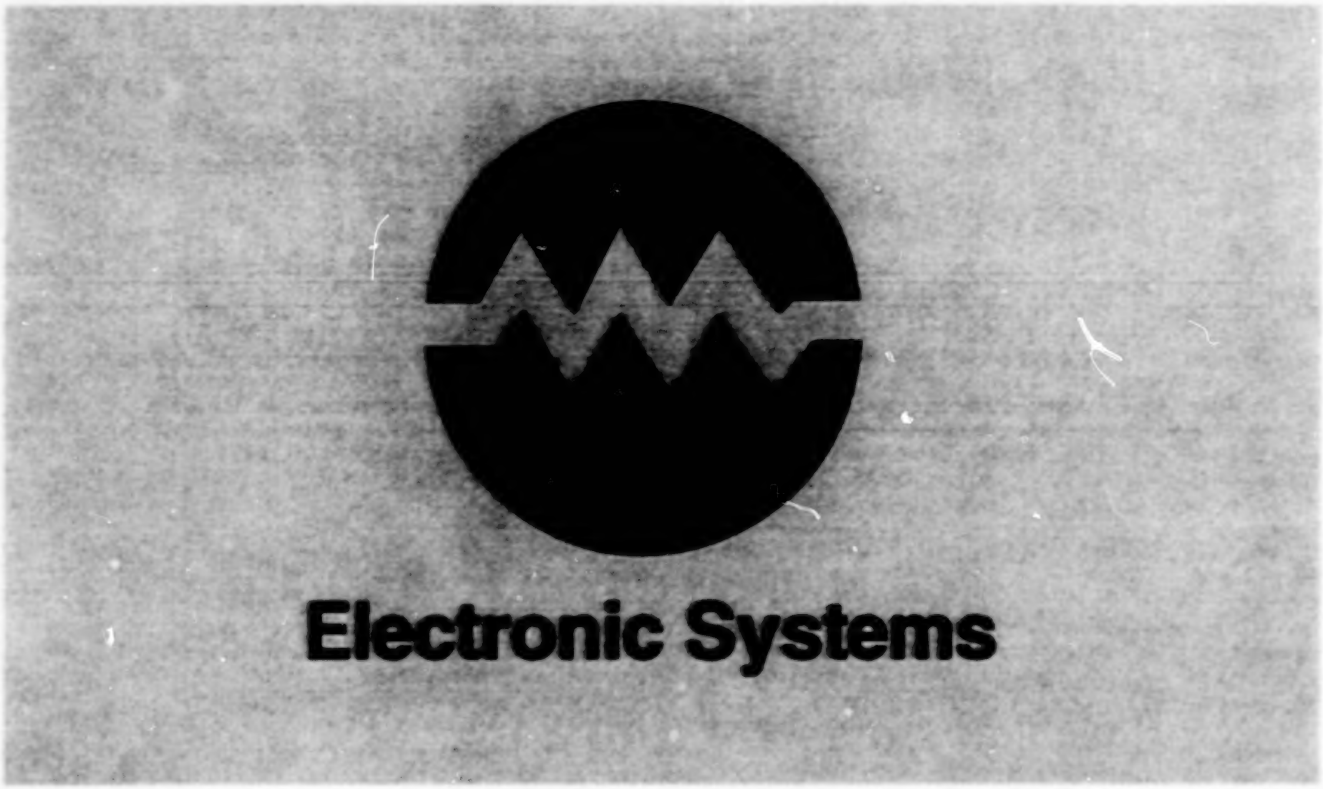

Hardware, Techniques, and Processes

Books and Reports

BLANK PAGE

Algorithm for Equalizing Rectangular Signal Constellations

For rectangular constellations, performance exceeds that of an older algorithm.

NASA's Jet Propulsion Laboratory, Pasadena, California

A rectangular-constellation-based blind-equalization (RECBEQ) technique implemented by a real-time, recursive algorithm has been developed to improve the performances of radio receivers in recovering unknown signals that are modulated with digital information and that have been distorted in propagation by multipath channels and carrier offsets. The technique is so named because it is intended specifically to enable the equalization of large-order rectangular signal constellations; for example, that of quadrature amplitude modulation (QAM).

Blind equalization provides for the recovery of unknown signals via a finite-dimensional linear projection of a channel output data vector; namely,

$$z_n = \sum_{i=0}^{L-1} w_i y_{n-i}$$

where z_n is the complex output sample from the blind equalizer at the nth sampling interval, w_i is the ith of L blind-equalizer coefficients, and y_j is the jth complex sample from the unknown channel. The latter sample can be expressed as a convolution of the sampled channel impulse response f_k with an unknown sequence of independent and identically distributed source symbols a_j; that is,

$$y_j = \sum_k f_k a_{j-k}$$

This equalization process is said to be "blind" because the w_is are derived from available channel output data only, without knowledge of either the transmitted signal waveform or the linear channel.

The present blind-equalization technique belongs to a class of such techniques in which the w_is are chosen to maximize or minimize objective functions (e.g., cost functions). The objective function for this technique is derived from a uniformly most powerful (UMP) scale-invariant hypothesis test between factored (rectangular) generalized Gaussian distributions. The net result of the derivation is the following time-recursive equation for updating the blind-equalizer coefficients:

$$w_k(n+1) = w_k(n) - \beta_{rect}\{(|z_{xn}|^{s-2} z_{xn} + j|z_{yn}|^{s-2} z_{yn}) - R_{Orect} z_n\} y^*_{n-k}$$

where β_{rect} is a positive "step size" which controls the rate of adaptation (smaller values of β_{rect} result in lower adaptation rates); the subscripts x and y denote the real and imaginary parts, respectively, of the affected quantities; s is a positive constant, greater than 2, which helps determine the steady-state performance of the equalizer (larger values of s yield lower steady-state adaptation noise but result in greater implementation complexity and greater sensitivity to additive receiver noise — it has been observed that $s = 8$ provides a good tradeoff between algorithm adaptation noise in steady state and sensitivity to additive receiver noise); R_{Orect} is a positive constant which controls the scale of the equalized constellation at convergence and is given by:

$$R_{Orect} = 2E|a_x|^s / E|a|^2$$

and $E()$ is the expectation operator. The equation for $w_k(n+1)$ converges rapidly for input rectangular constellations distorted by multipath.

When residual carrier offsets are present, the receiver must also include a data-directed phase-locked loop (PLL). Part of the figure depicts a conventional receiver architecture that incorporates a data PLL along with an older blind equalizer of a type called "CMA" (constant-modulus algorithm). The equalizer output is phase-corrected ("derotated") by the PLL output, which is driven by symbol decisions based on the phase-corrected equalizer output. This architecture is viable because the CMA is not affected by phase rotations of the input signal constellation, and therefore phase correction can occur downstream from the CMA equalizer.

Unlike the CMA, the RECBEQ algorithm is sensitive to the phase orientation. Extensive tests have revealed that the RECBEQ algorithm can acquire a rotating rectangular constellation, but not at the same level of precision that would be achieved if the constellation were static. This finding led to the development of the modified architecture, also shown in the figure. Here, the input to the RECBEQ

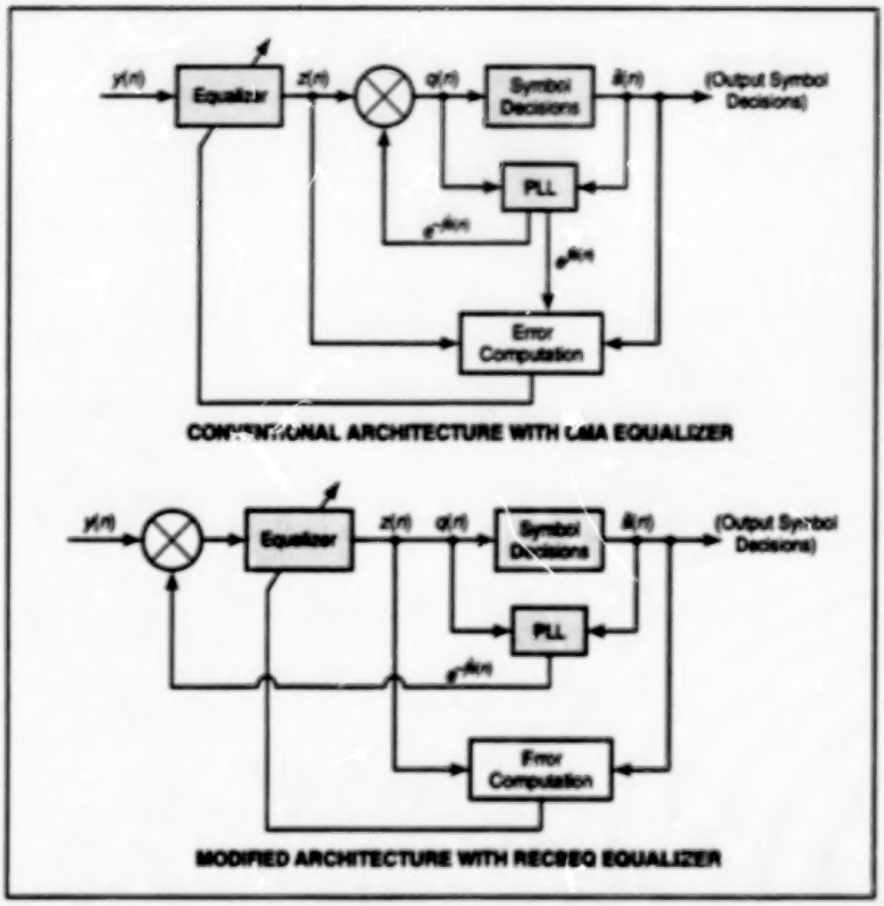

These Two Receiver Architectures effect joint blind equalization and carrier recovery. The equalizer and the PLL are connected in different ways in the conventional receiver architecture based on the CMA and the modified receiver architecture based on the RECBEQ algorithm.

equalizer is phase-corrected by the PLL output, which again, is driven by symbol decisions based directly on the equalizer output. In this architecture, the RECBEQ initially equalizes the rotating constellation to such an extent that the PLL can lock up and finalize the joint equalization/carrier-recovery process.

Results of computational tests show that for rectangular constellations, the RECBEQ algorithm converges much more quickly, to lower-noise solutions, than does the CMA. For other, more-rounded constellations [e.g., those of *M*-any-phase-shift keying (MPSK)], the CMA performs better. Computationally, both algorithms are comparable.

This work was done by Edgar Satorius of Caltech and James Mulligan of TASC for **NASA's Jet Propulsion Laboratory**. *Further information is contained in a TSP [see page 1].*
NPO-20324

Study of Mixed-Norm Controllers for Suppressing Vibrations

A report describes a study of nominal-performance (H_2), robust-performance (μ-synthesis), and mixed H_2/μ methods for designing fixed-order controllers applied to an active-tendon control system for suppressing seismic vibrations in a structure. The study involves an application of advances in control theory discussed in "Mixed-Norm Design of Fixed-Order Controllers" (MFS-26404), *NASA Tech Briefs*, Vol. 20, No. 5 (May 1996), page 91. The mathematical model of the structure in the study includes a parametric uncertainty representative of uncertainty in the frequency of each structural vibrational mode within the control bandwidth, plus an additive uncertainty to provide stability in the presence of unmodeled high-frequency modes. The sensitivity of H_2 design to unmodeled dynamics and parametric uncertainty is evaluated for a range of controller levels of authority. Next, μ-synthesis is applied to design full-order compensators that are robust to both unmodeled dynamics and parametric uncertainty. Then some designs of mixed H_2/μ compensators are optimized for 6th order. These mixed-norm designs are found to offer performance levels of H_2 designs, plus robust stability levels of μ designs. It is shown that mixed-norm design enables the use of higher levels of control authority for which H_2 designs are destabilizing.

This work was done by Mark S. Whorton of **Marshall Space Flight Center** *and Anthony J. Calise and C.-C. Hsu of the Georgia Institute of Technology. To obtain a copy of the report, "A Study of Fixed Order Mixed Norm Designs for a Benchmark Problem in Structural Control," see TSP's [page 1].*
MFS-27331

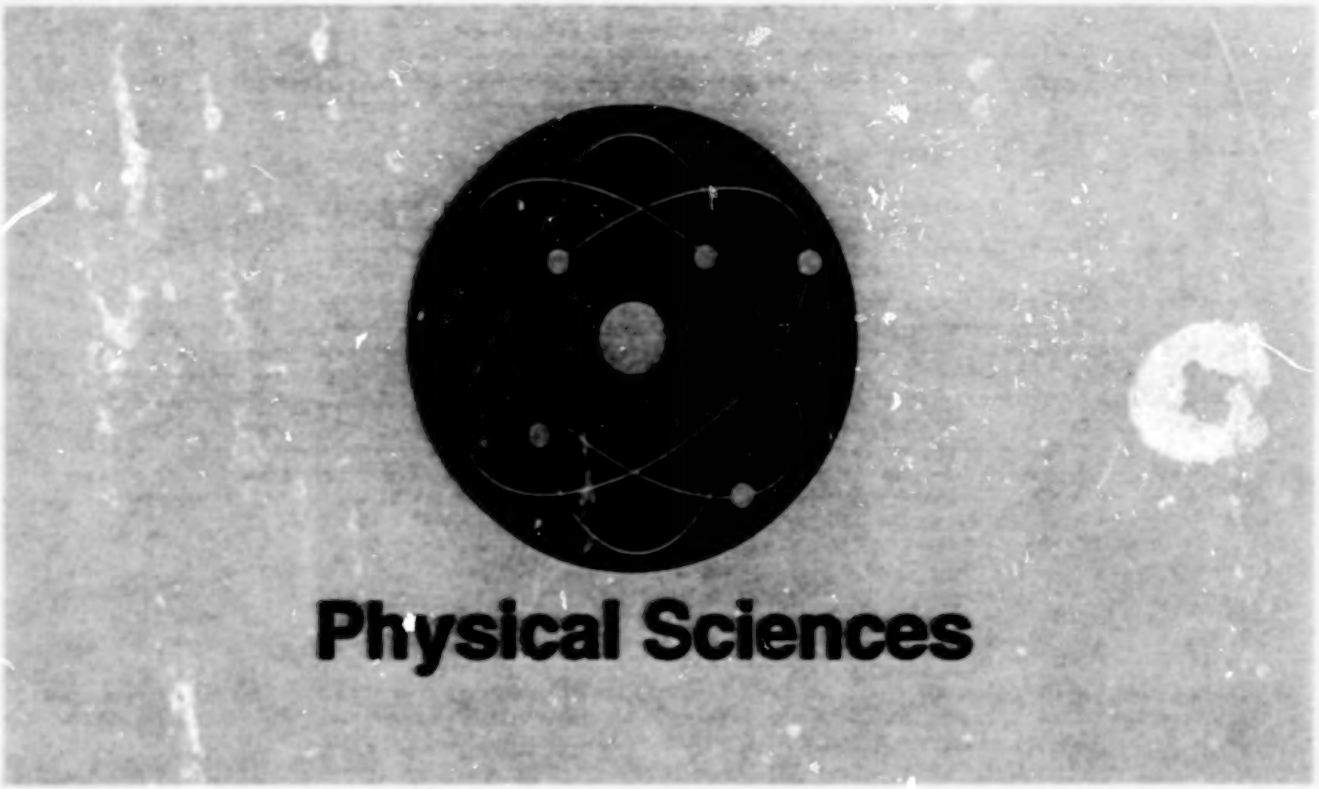

Physical Sciences

Hardware, Techniques, and Processes

Books and Reports

BLANK PAGE

Model of a Drop of O_2 Surrounded by H_2 at High Pressure

This model accounts for complex phenomena that are not represented in older models.

NASA's Jet Propulsion Laboratory, Pasadena, California

A mathematical model has been developed to predict the behavior of an isolated drop of a first fluid surrounded by a second fluid, under quiescent conditions at supercritical temperature and pressure. The model has been specialized to represent the behavior of a drop of liquid oxygen surrounded by hydrogen under supercritical conditions like those encountered in a rocket-engine combustion chamber. According to plans, this model will eventually be combined with other models to form a comprehensive model for the behavior (including combustion) of hydrogen and oxygen in a rocket-engine combustion chamber.

None of the related conventional mathematical models of the behavior of oxygen could represent the complex phenomena that occur in a rocket-engine combustion chamber. The conventional models are based, variously, on empirical correlations or on physics under subcritical conditions. The common weakness of the conventional models is failure to represent the physics under supercritical conditions.

The present model incorporates physics from first principles. It is based on fluctuation theory that incorporates equations for the conservation of momentum, mass for each molecular species, and enthalpy. The advantage of the theory is that it inherently accounts for nonequilibrium processes and naturally leads to the most general fluid-dynamical equations in which the heat flux and the partial molar fluxes are related to thermodynamic quantities (e.g., temperatures and chemical potentials). The relationships among these quantities are expressed using transport (diffusion)-matrix formulation. This formulation includes the Soret effect (transport of species due to thermal gradients) and the Dufour effect (transport of heat due to gradients in concentrations of species). The conservation equations are coupled with a law of kinetics for mass release, with equations of state, and transport coefficients that are accurate over the subcritical and adjacent supercritical ranges for both fluid oxygen and hydrogen.

The Soret and Dufour effects, along with thermodynamic nonequilibrium effects, are not taken into account in the conventional models. The inclusion of these effects in the present model results in modifications of length scales for heat and mass transfer, with important consequences for designing combustion chambers.

Numerical results obtained using this model show that under supercritical conditions, the behavior of the liquid-oxygen/hydrogen system is one of slow diffusion. The temperature profile relaxes fastest, followed by the density profile and then by the mass-fraction profile (see figure). An effective Lewis number estimated according to the theory described in the following article is found to be about 40 times the traditional Lewis number. Parametric studies reveal that gradients increase with increasing drop size, increasing pressure, or decreasing temperature; the practical consequence of this finding is that increased turbulence is needed to mix the hydrogen and oxygen at increased pressure.

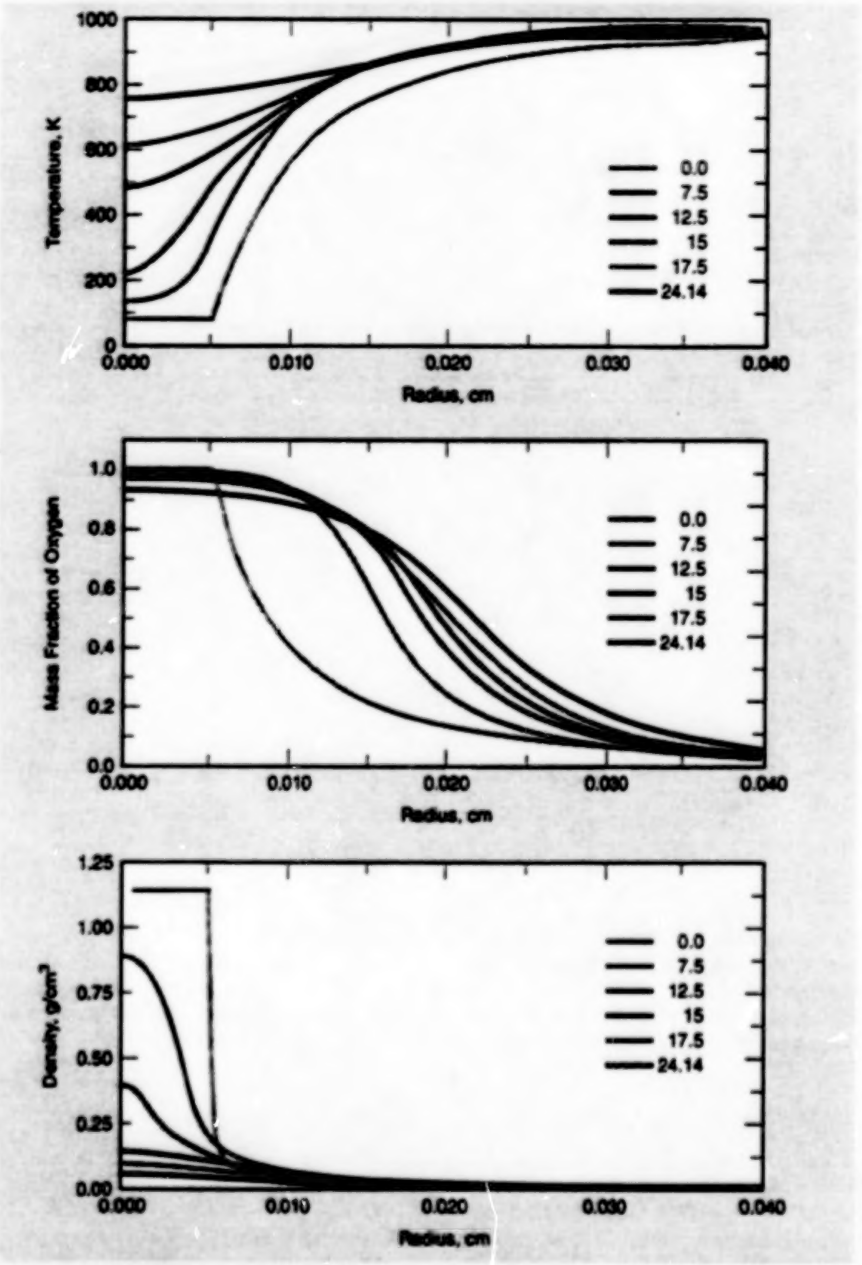

These Spatial Variations of temperature, mass fraction of oxygen, and mass density at various times were calculated by use of the model for an initial liquid-oxygen drop radius of 50 μm, a sphere-of-influence radius of 1 mm, an initial drop-surface temperature of 100 K, an initial temperature of 1,000 K at the edge of the sphere of influence, and a pressure of 20 MPa. The times are indicated on the graphs in milliseconds.

This work was done by Josette Bellan and Kenneth Harstad of Caltech for **NASA's Jet Propulsion Laboratory.** *Further information is contained in a TSP [see page 1].*

NPO-20220

The Lewis Number Under Supercritical Conditions

An effective Lewis number differs from the traditional Lewis number.

NASA's Jet Propulsion Laboratory, Pasadena, California

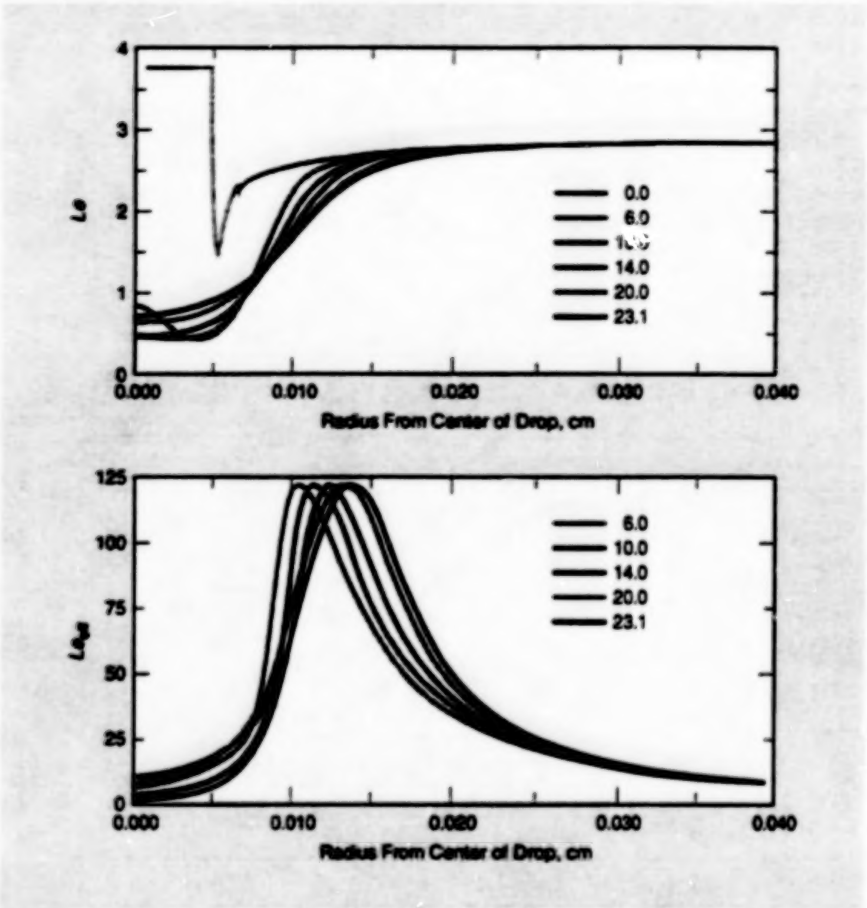

The Effective Lewis Number (Le_{eff}) and the Traditional Lewis Number (Le) were calculated at various times for isolated liquid-oxygen drop with an initial radius of 50 μm, a sphere-of-influence radius of 1 mm, an initial drop-surface temperature of 100 K, an initial temperature of 1,000 K at the edge of the sphere of influence, and a pressure of 80 MPa. The times are indicated on the graphs in milliseconds.

An effective Lewis number has been defined for two-fluid mixtures under conditions of (1) supercritical temperature and pressure and (2) large gradients of temperature and composition. The Lewis number is a measure of the ratio between characteristic lengths for diffusion of heat and diffusion of mass. The traditional definition of the Lewis number for a fluid is straightforward under subcritical conditions, in which the molar flux depends only on mole-fraction gradients and the heat flux depends only on the temperature gradient. Under supercritical conditions, the traditional definition of the Lewis number does not account for additional heat- and mass-transfer effects and thus leads to inaccurate estimates of heat- and mass-transfer scales. Accurate estimates of these scales are needed for designing combustors that operate under supercritical conditions; for example, combustors in rocket, gas turbine, and Diesel engines.

The need for an effective Lewis number (as distinguished from the traditional Lewis number) becomes apparent in the context of the fluctuation-dissipation theory described in the preceding article. In that theory, the Soret and Dufour effects are described by terms that include the off-diagonal elements of the transport matrix. The differential operators and equations for mass fractions and temperature are coupled through the off-diagonal elements in that the diffusion terms in each equation include derivatives of both dependent variables. This coupling through the off-diagonal elements prohibits a simple definition of diffusion length scales for heat and mass transfer and represents additional contributions to heat and mass transfer that are not considered in the traditional Lewis number. These observations suggest the need for an effective Lewis number that is valid under general (including supercritical) conditions.

The traditional Lewis number relates the diffusion lengths of the mass fractions and temperature as given by the coefficients of the diffusive terms. In the classical situation in which the traditional Lewis number is defined, the differential operators for mass fractions and species are uncoupled, and so the diffusion terms in the differential operators can be expressed as the product of a diagonal matrix and a spatial derivative. In order to be able to define an effective Lewis number in the general case, one must find equivalent variables for which the matrix of the differential equations assumes a diagonal form.

Given the complexity of the equations, a simple, accurate combination of variables cannot be found *a priori*. Therefore, a solution was sought for the special case of a drop of liquid (e.g., liquid oxygen) surrounded by a gas (e.g., hydrogen) under simplifying assumptions of (1) a boundary-layer spatial variation under subcritical conditions that exist in a thin radial interval at the surface of the drop and (2) quasi-steady behavior. The adoption of this special case makes it possible to define equivalent variables in the forms of linear combinations of the temperature and the mass fraction of one species, that yield the desired decoupling between differential equations for temperature and mass fractions.

Numerical results from calculations for binary fluid systems, variously involving isolated or interacting fluid drops, show that the effective Lewis number can be as much as 40 times the traditional Lewis number, and that the spatial variations of the two numbers are different (see figure). Thus, the traditional Lewis number cannot be relied upon to give even a qualitatively correct approximation of heat- and mass-transfer scales under supercritical conditions.

This work was done by Josette Bellan and Kenneth Harstad of Caltech for **NASA's Jet Propulsion Laboratory.** *Further information is contained in a TSP [see page 1].*

NPO-20256

Model of Interacting O_2 Drops Surrounded by H_2 at High Pressure

This model accounts for collective behavior, which affects stability or instability of combustion.

NASA's Jet Propulsion Laboratory, Pasadena, California

A mathematical model has been developed to predict the behavior of mutually interacting drops of a first fluid surrounded by a second fluid, under quiescent conditions at supercritical temperature. The model has been specialized to represent the behavior of drops of liquid oxygen surrounded by hydrogen under supercritical conditions like those encountered in a rocket-engine combustion chamber.

The drops of liquid oxygen are formed by atomization from jets of liquid oxygen. There is considerable experimental evidence that the atomization process forms the drops in clusters, and that the drops interact within each cluster. The interaction among drops affects the stability of combustion process. Therefore, a model like the present one is needed for designing combustors, and for analyzing and controlling their operation.

The situation represented by the present interacting-drop model is that of a cluster of a finite number of drops of one fluid (which could be liquid oxygen) immersed in another fluid (a dense gas that could be hydrogen). All the drops are assumed to be spheres of same radius, and each drop is assumed to reside in a fictitious sphere of influence with a radius equal to half the distance to the nearest neighbor drop in the cluster. The interstitial region between the spheres of influence is assumed to be uniform and quiescent with respect to the cluster. Each sphere of influence contains one drop and its surrounding fluid, and has fixed mass; this means that the sphere of influence expands or contracts in response to variations in temperature.

The behavior of a drop within its sphere of influence is represented by the isolated-drop model described in the first of the two preceding articles — "Model of a Drop of O_2 Surrounded by H_2 at High Pressure" (NPO-20220). The interactions among drops and the resulting collective behavior of the drops are represented by using equations for the conservation of total mass, conservation of the mass of each fluid, and conservation of energy in the interstitial region to establish boundary conditions for the spheres of influence. Transfers of heat and mass to the cluster are modeled via a Nusselt-number formulation.

Numerical results from calculations for the liquid-oxygen/hydrogen system (see figure) show that the behavior of a cluster is insensitive to variations of the Nusselt number over 3 orders of magnitude. The results also show that at fixed pressure, the accumulation of oxygen in the interstitial region increases with decreasing distance between drops. At fixed initial distance between drops, the gradients of dependent variables become increasingly smeared as pressure increases; this behavior is qualitatively the opposite of that observed for isolated drops. From these observations it is inferred that clusters of drops might be desirable in supercritical combustion because they aid mixing of reactants.

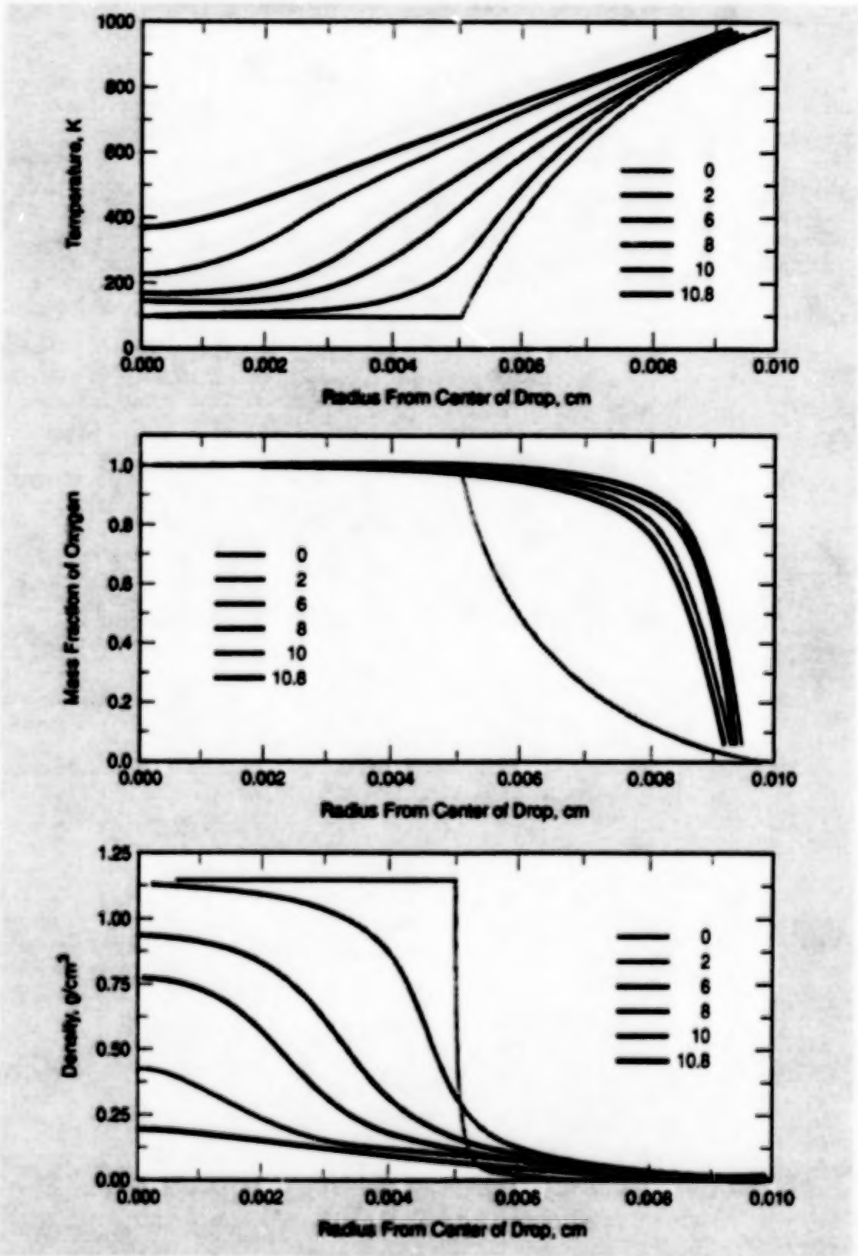

These Plots Show Numerical Results from one of a number of example calculations performed by use of the model. The basic parameters in this example were an initial liquid-oxygen drop radius of 50 μm, initial sphere-of-influence radius of 100 μm, initial cluster radius of 2 cm, equivalent Nusselt number of 100, initial drop-surface temperature of 100 K, initial temperature of 1,000 K at the edge of the sphere of influence and outside the cluster, pressure of 20 MPa, and no oxygen outside the cluster. Times are indicated on the graphs in milliseconds.

This work was done by Josette Bellan and Kenneth Harstad of Caltech for **NASA's Jet Propulsion Laboratory.** *Further information is contained in a TSP [see page 1].*

NPO-20257

Two Techniques for Controlling Altitudes of Lifting Balloons

Multiple ascents and descents on long flights would be possible.

NASA's Jet Propulsion Laboratory, Pasadena, California

SOLAR BALOON LANDING ON MARS

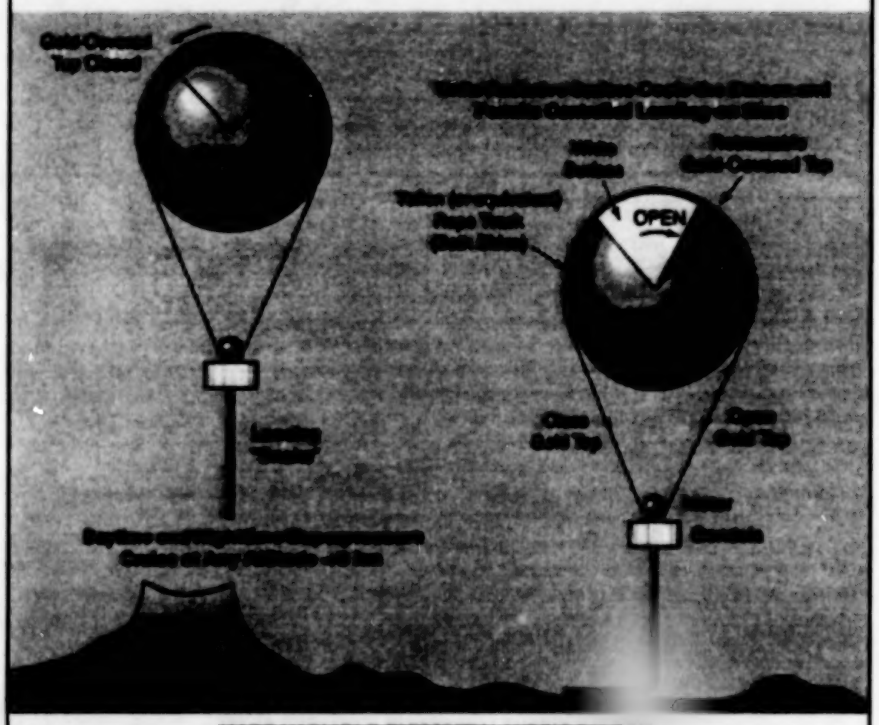

MARS VARIABLE EMISSIVITY LANDING BALOON

Two Techniques can be used to control the altitudes of robotic lifting balloons. A solar hot-air balloon uses vents (shown on top of the balloon) to control its buoyancy; another balloon uses variable-emissivity surface to control its buoyancy.

Two techniques have been proposed (see figure) for controlling the buoyancies and thus the altitudes of robotic lifting balloons (aerobots) that would carry scientific instruments for exploration of Mars. Buoyancy-control techniques other than these have been, variously, used on Earth and/or proposed for use in exploring planets other than Mars, but have been found inadequate for providing the requisite altitude control in the thin Martian atmosphere and at the low nighttime Martian surface temperature. The proposed techniques could also be used on Earth; for example, for carrying instruments to perform surveillance, monitor weather, or measure pollution.

The first proposed technique pertains to solar hot-air balloons. The concept of solar hot-air balloons is not new in itself; toy solar-heated balloons have been commercially available for years, and experiments on solar-heated aerobots for planetary exploration have been performed in recent years. The novel aspect of the proposed technique lies in the addition of controllable vents to the tops of the solar-heated balloons, similar in function to the controllable vents on commercial combustion-heated balloons. By letting out heated air from a balloon, one could reduce buoyancy to obtain descent. Conversely, one could close the vent so that as solar heating continued, buoyancy would increase, causing the balloon to ascend. In the case of remote and/or automatic control, the vent could be, for example, a motorized, balanced butterfly valve similar to a carburetor air valve. Of course, the balloon would have to land at night. Using this technique, multiple controlled soft landings and re-ascents have occurred in test flights in the Mojave Desert and off Southern California's Catalina Island.

Another unusual advantage of solar-heated balloons on Mars is the ability to use the balloon instead of retro-rockets, to soft-land payloads. The balloons not only cost much less, but they can increase useable landed payloads from under 10 percent (*Pathfinder*) to about 50 percent of total atmospheric entry mass.

The second proposed technique would be implemented on balloons filled with low-density gases (e.g., helium) at slight overpressures. This technique would provide altitude control during the night as well as the day. A balloon would be equipped with a variable-emissivity surface to control its internal temperature, and thus its buoyancy, by controlling the balance of thermal radiation among the balloon, the ground below, and the sky above. In the Mars case, for example, a balloon might be coated with gold, and equipped with a gold-coated top cover that could be retracted to expose a white top surface to the radiant cooling of deep space. Thus, retraction of the cover would cause buoyancy to decrease.

This work was done by Jack A. Jones of Caltech for **NASA's Jet Propulsion Laboratory**. *Further information is contained in a TSP [see page 1].*
NPO-20360

Composing Flow-Streak Images From Colorized Particle Images

Colors assist in visualization of flows and provide additional information on directions and times.

Lewis Research Center, Cleveland, Ohio

A method for making a flow visible in a plane and determining in-plane velocities involves the digitization and digital processing of a sequence of monochrome video images of particles entrained in the flow. The particle-laden flow passes through a sheet of laser or lamp light in the plane, which is oriented perpendicularly to the viewing direction. As described thus far, this method involves the use of techniques that have become common in the flow-visualization art and that have been described in numerous articles in *NASA Tech Briefs*. The unique aspects of the present method originate in the following critical digital image-processing steps:

- In a grey-scale preprocessing stage, each image is enhanced to visually separate the particles from the background. Preprocessing is accomplished by one or more techniques that can include simple semithresholding, percentile semithresholding, and/or a top-hat morphological transformation. The choice of preprocessing technique(s) depends on the quality of the original image.
- A different known false color is assigned to each video frame in the sequence, and the frames are superimposed into a single composite, time-lapse color video image. The information from each frame in the composite image can be distinguished by color from the information from the other frames and thereby identified by color as having been recorded at a unique observation instant in a sequence of observation (video-frame) instants.

The color sequence must be chosen so as not to give rise to aliases in a hue subset. For example, hues of green, yellow, and red could result in a yellow spot for both a particle that was stationary for the full exposure and a particle that just moved through the light sheet during the "yellow" time step. These yellow spots would be indistinguishable. The use of a color sequence from magenta to cyan obviates this "yellow" ambiguity.

In older methods of streak photography and time-lapse imaging, there is no way to determine which way a particle moved along its image streak; there is also no way to determine whether a particle remained in the light sheet during the entire observation time or, alternatively, when it entered and left the light sheet. In the present method, the color of each streak changes from one end to the other in the known sequence, giving a clear indication of the direction of the motion of the particle. If the entire sequence of colors is present in a streak, then the particle can be assumed to have remained within the light sheet during the entire sequence of frames; if any colors are missing, then the times when the particle entered and left the light sheet can be determined from the colors at the ends of its streak image. The missing-color information also provides a qualitative indication of the degree of flow in directions other than in the illuminated plane.

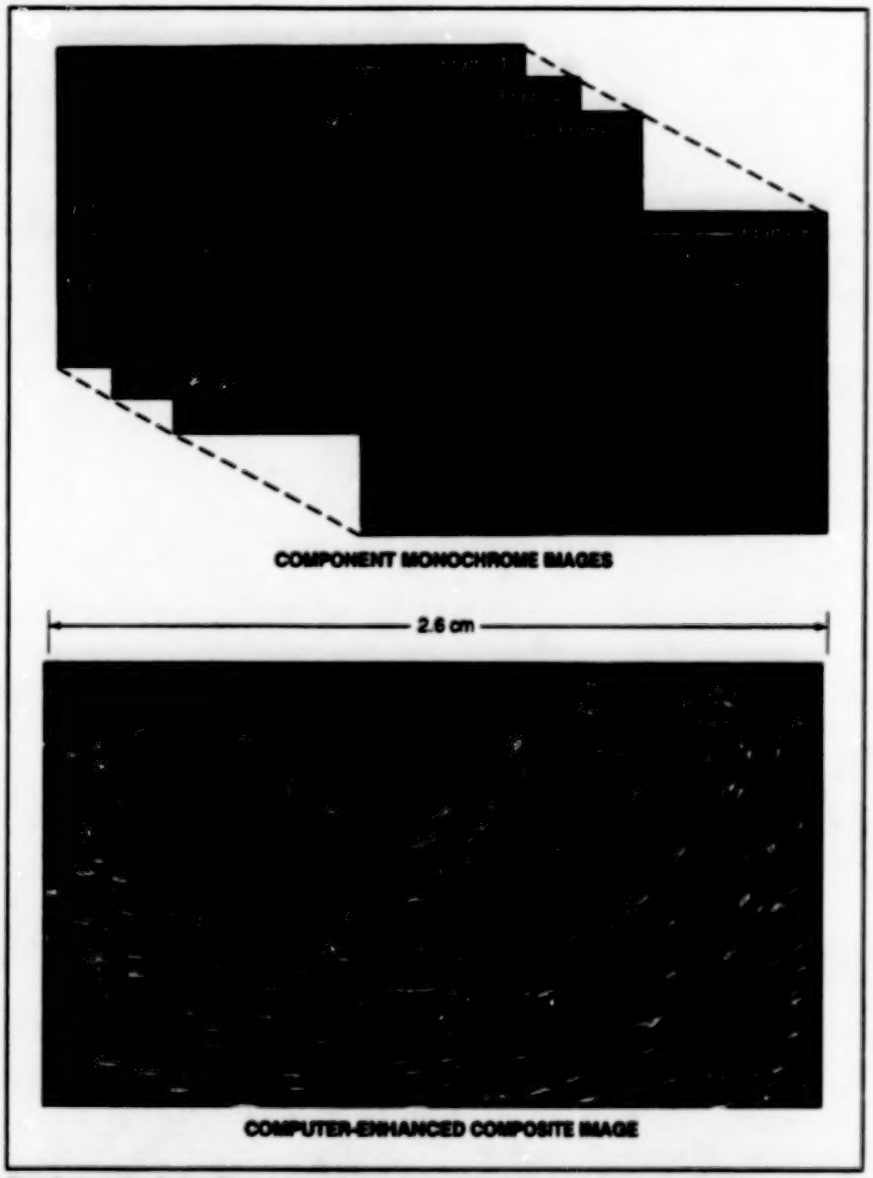

This Composite Color Time-Lapse Image was made from a sequence of eight false-color versions of original video frames that show particles entrained in a flammable liquid that was stirred into a vortex by a flame (not shown) moving to the right across the top. The border of each original frame shows the color assigned to that frame in the composite image. The eight frames were recorded sequentially during a total elapsed time of 0.267 second.

The average in-plane speed of a particle can be computed as the length of its image streak divided by the total elapsed time of the frame sequence. In analyzing streaks to extract velocities (speeds and directions), one might wish to reject streaks with missing colors on the ground that the corresponding particles did not spend the full elapsed time in the light sheet. Optionally, one could use these streaks, provided that the times used in the denominators for computing speeds are the par-

tial elapsed times determined from the missing colors.

Unlike in conventional streak photography, there is no need for *a priori* knowledge of exposure times. Different parts of an image can be processed differently, if necessary. A composite exposure time can be chosen after a test.

By use of a digital frame recorder, images processed by this method can be rerecorded onto video tape to make digital movie sequences that can be viewed on computer workstations. These movies show moving particle streamlines (or pathlines in unsteady flows), rather than only moving particles; in so doing, the movies make it much easier to visualize the flows.

This work was done by Fletcher J. Miller of Case Western Reserve University and Mary B. Vickerman and Howard D. Ross of **Lewis Research Center**. *Further information is contained in a TSP [see page 1].*

Inquiries concerning rights for the commercial use of this invention should be addressed to NASA Lewis Research Center, Commercial Technology Office, Attn: Steve Fedor, Mail Stop 4–8, 21000 Brookpark Road, Cleveland, Ohio 44135. Refer to LEW-16381.

Ultrasonic Profiling of an Object

An additional use for an ultrasonic scanning apparatus has been found.

Goddard Space Flight Center, Greenbelt, Maryland

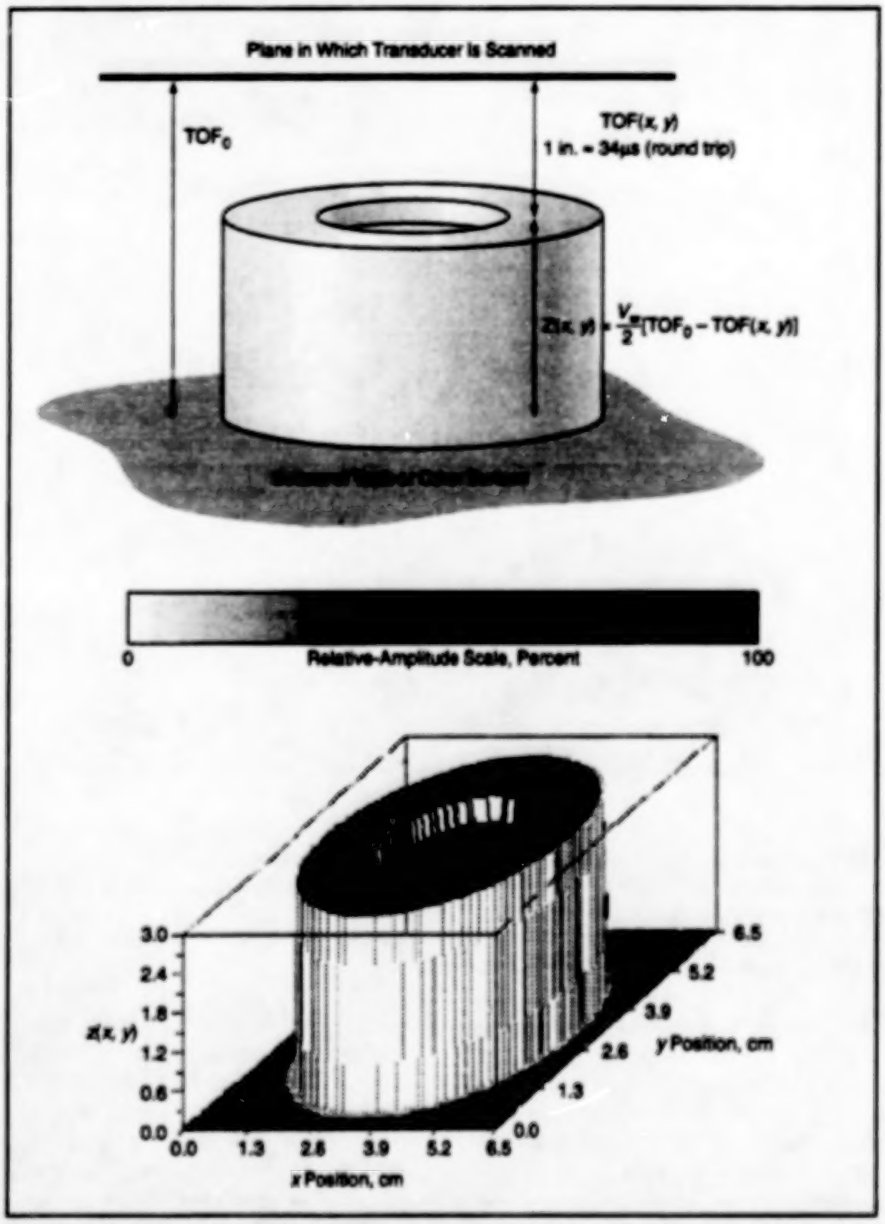

The Top Surface of the Object can be profiled or mapped by use of the time of flight of an ultrasonic signal as a function of horizontal position *x,y*.

A computer-controlled ultrasonic C-scan instrumentation system that was developed primarily for use in finding defects inside solid material specimens can also be used to obtain three-dimensional profiles of the top surfaces of such specimens. In some applications, ultrasonic profiling by use of this system might be an attractive alternative to profiling by use of calipers, linear variable-differential transformers, coordinate-measuring machines, laser profilometers, and other instruments.

The present ultrasonic instrumentation system was described in "Apparatus for Advanced Ultrasonic C-Scan Imaging" (GSC-13524), NASA Tech Briefs, Vol. 21, No. 4 (April 1997), page 34. To recapitulate: The system includes an ultrasonic transducer that is scanned in a horizontal (*x,y*) plane and that is connected to an electronic pulser/receiver, a dual timing gate, a peak detector, and a universal timer. At each position *x,y* along the scan, the computer estimates the depth of any feature that reflects ultrasound, using the known or assumed speed of sound and the measured round-trip travel time (also called "time of flight," or "TOF" for short) of the ultrasonic signal. The peak detector operates with a time gate chosen so that its output indicates the amplitude of the signal reflected from the feature of interest at *x,y*. Once the scan has been completed, the computer processes the *x,y* scanning-position data and the associated depth and amplitude data into a single three-dimensional-appearing plot that shows both depth and amplitude as functions of *x* and *y*.

The figure illustrates the use of the system for profiling. An object to be profiled is placed on the bottom of a tank of water with the surface of interest facing upward. The transducer is immersed in the water so that its *x,y* scanning plane lies at a convenient height above the object. For the purpose of profiling, the TOF to measure is the round-trip travel time for ultrasound that originates at the transducer and that is reflected from the top surface of the object back to the transducer. Then the local height of the object is given by

$$Z(x,y) = (V_w/2)[TOF_0 - TOF(x,y)],$$

where V_w is the speed of sound in water, TOF_0 is the round-trip travel time observed when the object is not present or when the transducer is not over the object and is aimed at the surface on which the specimen sits, and TOF(x,y) is the round-trip travel time for position x,y.

This work was done by E. James Chem of **Goddard Space Flight Center.** *No further documentation is available.*
GSC-13911

Hybrid Acoustic/Electrostatic Levitation Apparatus

Conditions for experiments on growth of crystals, cells, and tissues can be highly controlled.

NASA's Jet Propulsion Laboratory, Pasadena, California

The figure schematically illustrates a developmental automated hybrid acoustic/electrostatic apparatus for levitating both electrically charged and electrically neutral liquid drops with sizes up to about 1 mm. The apparatus is particularly suitable for experiments on the growth of protein crystals from solution and on the growth of cells and tissues, all under controlled conditions. In addition to the obvious advantage of levitation for preventing the chemical and thermal contamination that accompanies contact between drops and external objects, this apparatus provides controllable rotation about a horizontal axis (for example, to reduce sedimentation). Moreover, the direction of rotation can be varied to randomize the effective direction of gravitation. Thus, on Earth, the apparatus is expected to provide some of the advantages of low gravitation for suppressing the buoyancy-induced flows that interfere with the growth of high-quality protein crystals and for reducing the adverse effects that gravitation exerts on some cell and tissue cultures.

An electrically neutral drop can be levitated acoustically. An electrically charged drop can be levitated electrostatically and/or acoustically. An important advantage of using both kinds of levitation is that if the acoustic field is used to produce rotation, the intensity of this field can be minimized, thereby minimizing disturbances in the drop. It has been conjectured that aerodynamic drag from acoustic streaming in the surrounding air is the physical mechanism through which the acoustic field exerts torque on the drop. The direction and amount of torque can be controlled by horizontal displacement of the acoustic transducer from its nominal central position under the acoustic reflector.

The apparatus allows optical access for observation, diagnosis, and process control. For example, optical diagnoses could be performed by imaging, light-scattering, and spectroscopic techniques. Temperature and humidity can be controlled and purity can be maintained by placing the apparatus in a closed chamber. A focused beam of light from a laser or other radiant source can be used for directional heating of a levitated drop.

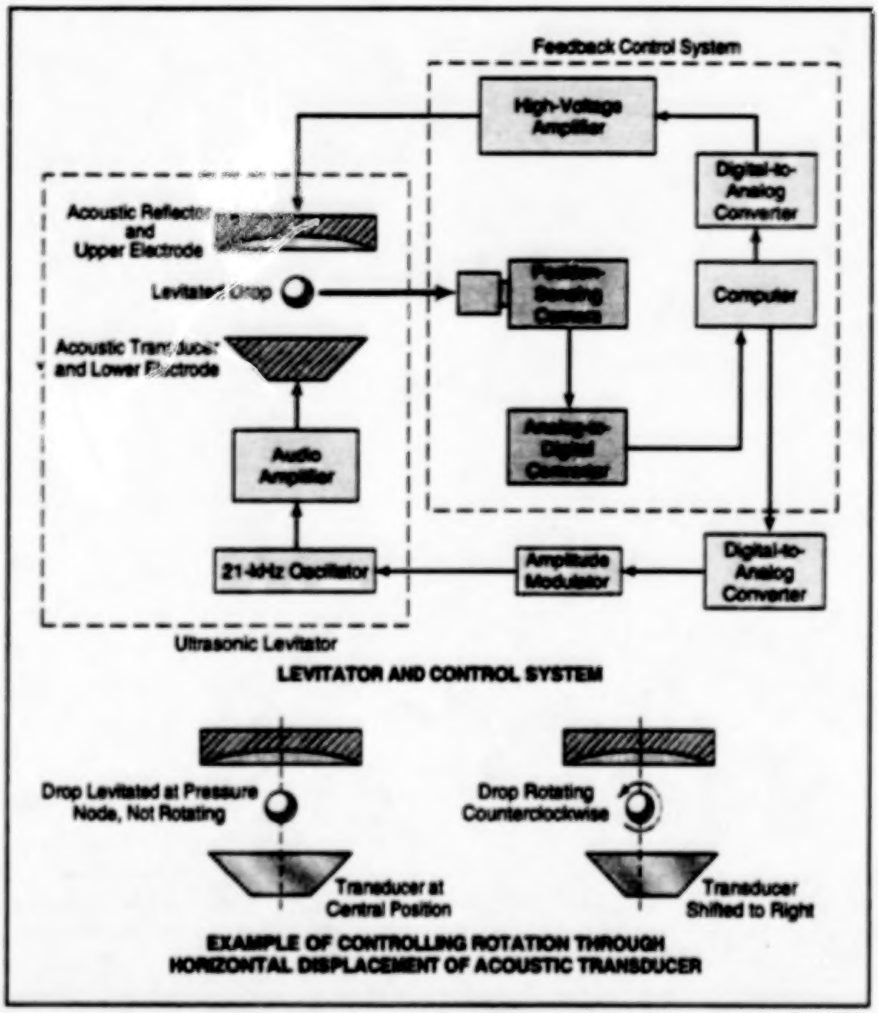

This Hybrid Acoustic/Electrostatic Levitation Apparatus provides relatively quiescent levitation under controlled conditions, plus optical access for observation, diagnosis, and process control.

This work was done by Eugene H. Trinh and Sang K. Chung of Caltech for **NASA's Jet Propulsion Laboratory.** *Further information is contained in a TSP [see page 1].*

In accordance with Public Law 96-517, the contractor has elected to retain title to this invention. Inquiries concerning rights for its commercial use should be addressed to

Technology Reporting Office
JPL
Mail Stop 122-116
4800 Oak Grove Drive
Pasadena, CA 91109
(818) 354-2240

Refer to NPO-20165, volume and number of this NASA Tech Briefs *issue, and the page number.*

Inflatable Fresnel Lenses as Concentrators for Solar Power

Primary advantages would be light weight and tolerance of shape errors.

Lewis Research Center, Cleveland, Ohio

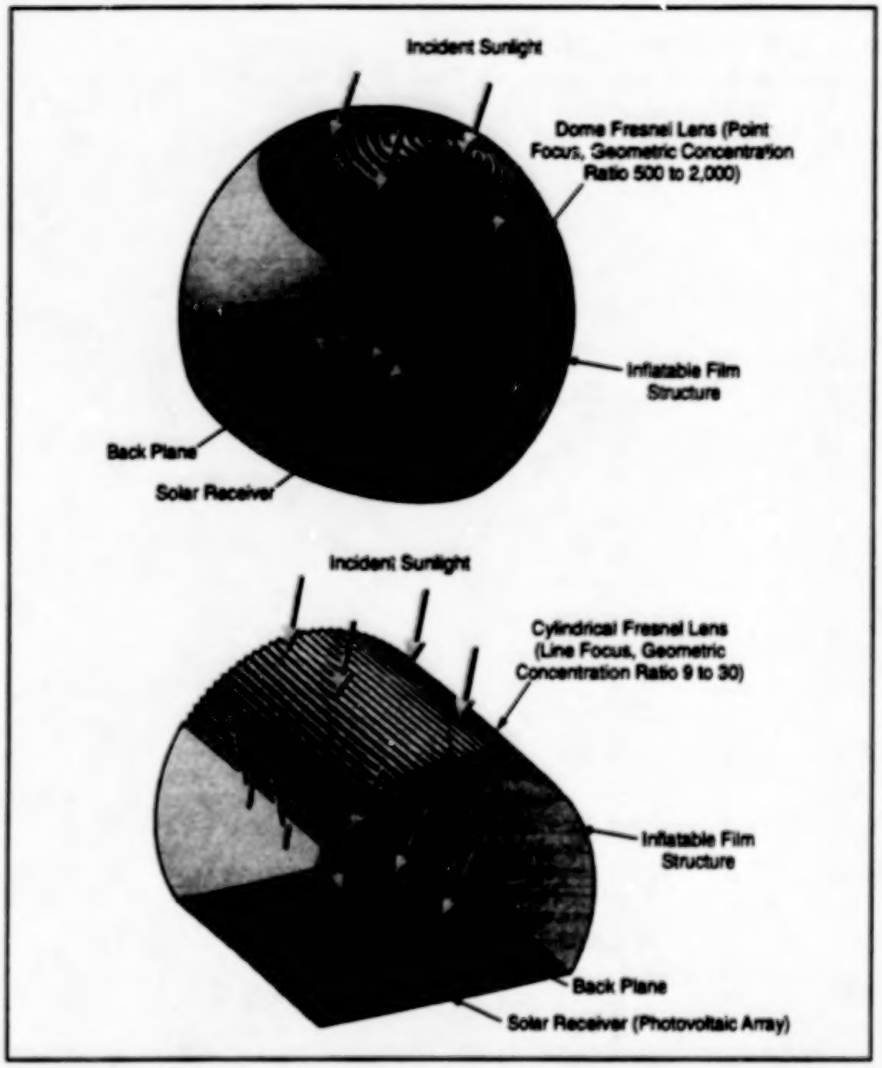

Figure 1. Fresnel Lenses would be supported on the interior surfaces of spherical and cylindrical balloons. The spatial intervals between Fresnel-lens prisms are greatly exaggerated in these views.

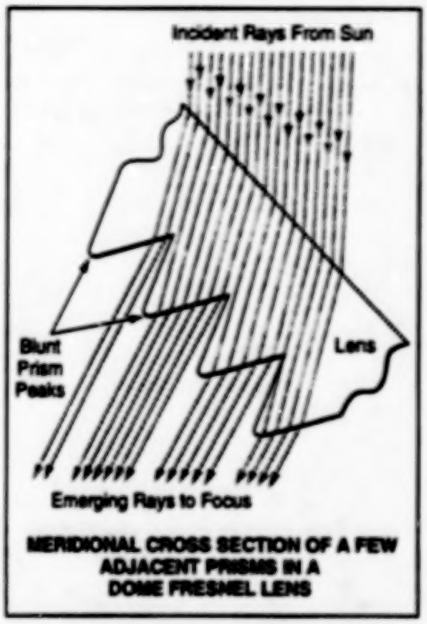

Figure 2. A Symmetrical-Refraction Design (in which the angle of incidence equals the angle of emergence) maximizes the tolerance to slope error in that it minimizes the deviation of the angle of refraction for a given slope error. An additional benefit of the configuration shown here is that the blunt prism peaks are tucked out of the ray paths and thereby prevented from scattering light.

Inflatable Fresnel lenses are being developed for use as optical concentrators in solar power systems. These lenses are of two types: dome (point-focus) lenses and cylindrical (line-focus) lenses (see Figure 1). Originally intended for supplying power to spacecraft, these lenses might also be adaptable to some terrestrial solar-power systems in cases in which optical aberrations caused by gravitational and wind-loading distortions of lens shapes could be tolerated.

The main structural element of a dome lens concentrator would be a spherical balloon. The balloon would be made of a polymer (e.g., polyethylene terephthalate) film about 12 μm thick, possibly coated with aluminum on both sides everywhere except in the dome lens region. The concentric prisms that constitute the Fresnel lens elements could be molded into a sheet that would be bonded to the inner surface of the balloon; typically, this Fresnel-lens sheet would be cast from clear silicone rubber and would be about 250 μm thick. In practice (at least initially) it could be desirable to approximate the desired spherical shape by assembling the balloon and Fresnel lens from gores. At a latitude chosen consistently with the focal length and the radius, the balloon would be anchored on a back plane that would support the solar receiver and would serve as a radiator for dissipating waste heat.

A paraboloidal dish reflector is the main competitor to an inflatable dome lens concentrator. The most obvious advantage of an inflatable dome Fresnel-lens concentrator is that a large concentrator surface can be established and maintained readily by inflating a lightweight balloon, whereas a paraboloidal dish rigid enough to maintain the required shape weighs considerably more. Another less obvious but equally important and concomitant advantage is that in comparison with a paraboloidal reflector of nominally equal area and relative aperture, a dome Fresnel lens can be made considerably more tolerant of shape error (see Figure 2); for a typical slope error at the outer edge of the lens, the spreading of the solar image is less than a hundredth of that caused by the same slope error at the outer edge of the reflector.

A cylindrical Fresnel-lens concentrator would be essentially a simplified, two-dimensional version of a dome Fresnel-lens concentrator. The dome Fresnel-lens concentrators would be well suited for applications in which there is requirement for aperture sizes of the order of meters for photovoltaic, thermophotovoltaic, and various types of thermal solar receivers. The cylindrical Fresnel-lens concentrators would be suitable primarily for aperture

widths of 5 to 10 cm for linear arrays of photovoltaic cells.

This work was done by Mark J. O'Neill and A. J. McDanal of ENTECH, Inc., for **Lewis Research Center**. *Further information is contained in a TSP [see page 1].*

Inquiries concerning rights for the commercial use of this invention should be addressed to NASA Lewis Research Center, Commercial Technology Office, Attn: Steve Fedor, Mail Stop 4–8, 21000 Brookpark Road, Cleveland, Ohio 44135. Refer to LEW-16662.

Wide-Angle, Open-Faced Retroreflectors for Optical Metrology

Multiple corner-cube reflectors would be arranged with common vertices.

NASA's Jet Propulsion Laboratory, Pasadena, California

Wide-angle, open-faced retroreflectors of a proposed type would be constructed by use of traditional corner-cube reflectors as building blocks. Wide-angle retroreflectors are needed in optical stellar interferometry, and in other branches of highly precise laser metrology; in particular, two- and three-dimensional triangulation. All of these applications involve the use of reference structures (e.g., optical trusses) and the use of retroreflectors that establish fiducial points on the structures.

Ordinarily, single hollow corner-cube reflectors would be preferred as retroreflectors because they are not wavelength-dispersive and, in principle, return flat wavefronts with no distortion. Unfortunately, the range of useful acceptance angles of a corner-cube reflector in a given plane is only about 60°; this precludes the use of a corner-cube reflector at a fiducial point where two or more optical paths are required to intersect at an angle or angles greater than about 60°. Some non-corner-cube retroreflectors offer wider angular ranges; for example, a hemispherical lens offers a range as wide as 180°, but the reflected wavefront is subject to spherical and other aberrations, wavelength dispersion, and wavefront distortion associated with thermal expansion of the lens material along the optical path.

The proposed solution is to assemble multiple corner-cube reflectors for each fiducial point, subject to the following requirements: The corner-cube reflectors in the assembly must be mounted in various orientations such that, collectively, they provide acceptance angles to accommodate all optical paths required to intersect at the fiducial point (one or more beams can hit each corner). To establish the single desired fiducial point, the reflectors must be aligned so that their reflective faces intersect at that point.

Different geometries with two, three, even four corners have been considered. For the needs of JPL's space interferometry mission and its testbed, a triple corner cube design has been adopted, with

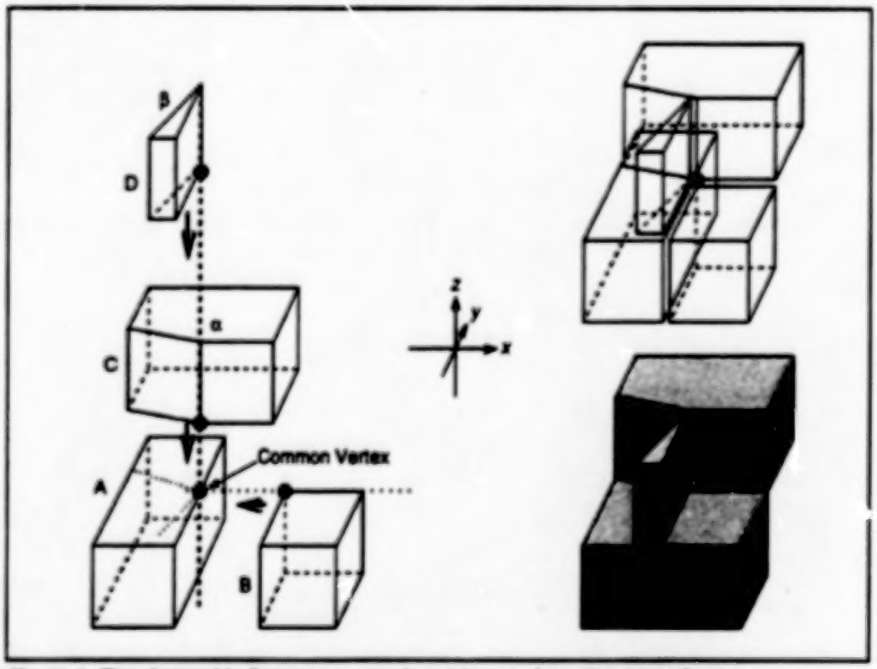

Figure 1. The Assembly Sequence uses four prisms to form the retroreflector.

Figure 2. A Prototype constructed at JPL is shown in this photograph.

a 30° wedge (see assembly sequence in Figure 1). A prototype has been successfully constructed in mid 1997, validating the concept of such a retroreflector and its manufacturability (see Figure 2).

The corner-cube reflectors would most likely be made from low-thermal-expansion glass prisms. The reflective corner faces would be polished flat to within 1/10 of a typical visible-light wavelength and coated for reflectivity. During assembly of the prisms to form the corners, special multiwavelength interferometric methods would be used to align the reflective faces to within arc seconds of the desired angles.

In practice, the fiducial point would have to be a virtual one, because it would not be possible to assemble multiple corner-cube reflectors with faces that continue, precisely, all the way into a common vertex. To enable assembly, it would be necessary to bevel at least some of the prisms, thereby leaving small gaps at the common vertex. If the bevels were made with custom polishing, then the gaps could be limited to < 50 μm. The quality of the reflected wavefronts would be limited only by the quality of the reflective faces and diffraction from the gaps.

This work was done by Edouard Schmidtlin of **NASA's Jet Propulsion Laboratory**. *Further information is contained in a TSP [see page 1].*

In accordance with Public Law 96-517, the contractor has elected to retain title to this invention. Inquiries concerning rights for its commercial use should be addressed to

Technology Reporting Office
JPL
Mail Stop 122-116
4800 Oak Grove Drive
Pasadena, CA 91109
(818) 354-2240

Refer to NPO-20174, volume and number of this NASA Tech Briefs issue, and the page number.

Low-Distortion Imaging Spectrometers

Distortion would be minimized by use of modified Offner optics.

NASA's Jet Propulsion Laboratory, Pasadena, California

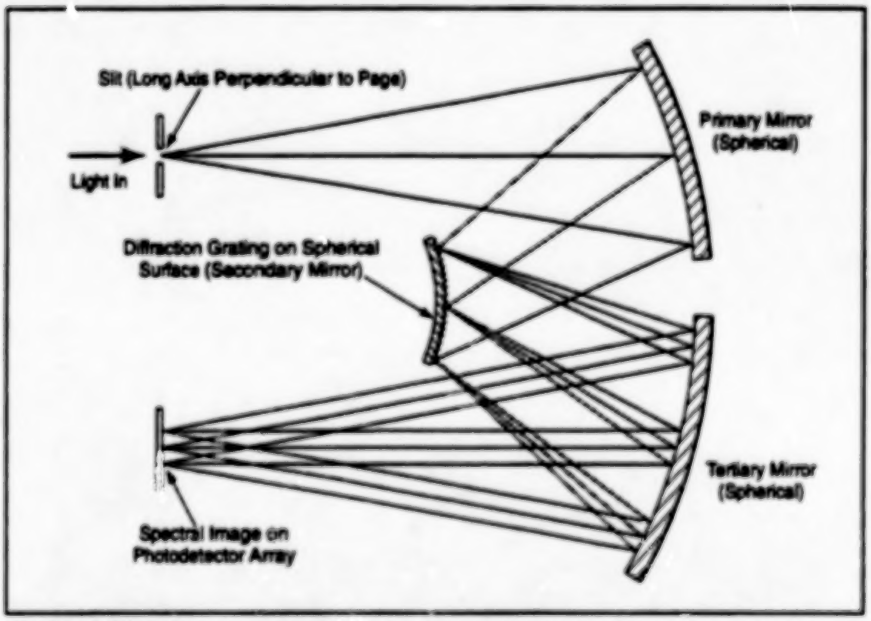

Modified Offner Spectrometer Optics can be optimized to minimize both spot size as well as spectral and spatial distortions.

"Pushbroom" imaging spectrometers of a proposed type would exhibit little or no distortion in either the spectral or spatial direction. These spectrometers would feature modified Offner optics, which afford a desirable combination of compactness and a high degree of optical correction. Although Offner optics have been used in some spectrometer designs, their potential for eliminating distortion does not appear to have been exploited.

A pushbroom spectrometer includes a rectangular photodetector array with pixels arranged in rows (parallel to a spatial axis defined by a straight slit) and columns (parallel to the spectral axis). Light enters the spectrometer through the slit. Each point or pixel along the slit corresponds to a point or pixel along one spatial axis in the scene under observation. Thus, each column of pixels gives a readout of the spectrum for one point or pixel on a line that crosses the scene. The term "pushbroom" arises because in an action reminiscent of a pushbroom sweeping a floor, the field of view is swept through the scene, along a line perpendicular to the slit, to acquire spectral readouts from all pixels in the scene.

Accurate calibration is crucial for the extraction of detailed quantitative information from the readouts. The difficulty of calibration is reduced considerably if (1) the monochromatic image of the slit is straight and parallel to the rows of the photodetector array at any wavelength and (2) the spectrum of any point along the slit is straight and parallel to the columns of the array. When these conditions obtain, the length of a monochromatic slit image and the length of the spectrum remain constant across the array. Deviations from these conditions are denoted as spectral and spatial distortion, or "smile" and keystone error.

Although it may seem obvious that the above types of distortions should be minimized, values of as much as 1 or 2 pixels have been accepted in previous spectrometer designs. Recent studies have shown that to preserve the integrity of spectral image data, one must limit smile to no more than a hundredth of a pixel, while similar stringent requirements apply to the keystone error as well as the variation of the pixel spectral response function. These requirements push accuracy and optical-correction requirements into a hitherto unexplored range, where, it turns out, a modified Offner configuration offers design solutions.

In a spectrometer of the classical Offner configuration, there are two concentric mirrors: a concave mirror and a convex mirror with twice the curvature of the concave one. The concave mirror is used twice, as both the primary and the tertiary mirror. A diffraction grating is deposited on the convex mirror. This optical system has a nominal magnification of –1. The system can provide good correction at high *f*

number (ratio of focal length to aperture diameter) and for low-dispersion gratings, while simultaneously limiting smile. But for lower *f* number and/or larger grating dispersion (which is often needed), it is normally found advantageous to have separate primary and tertiary mirrors (see figure), the curvatures and separations of which can be chosen independently in the design-optimization process.

The design-optimization process includes the use of a merit function based partly on spot size and partly on intersections of specific light rays with the image plane to characterize the centroids of ray distributions as indicators of smile. With that merit function, it has been found possible to control smile and keystone error to essentially arbitrary accuracy at the design stage, over a wide range of designs. These designs all involve centered mirrors with purely spherical surfaces (no aspherical terms), and no tilts. Tolerance analysis has revealed that manufacturability and alignment are within reason.

In controlling distortion and spot size simultaneously, it is important to use the appropriate grating order of diffraction; in particular, the simplest designs are usually obtained by use of the +1 order, for which the angle of diffraction is less than that of the 0 order. Diffraction gratings that would satisfy stringent requirements for low distortion could be fabricated on the convex mirrors by electron-beam lithography. The detailed grating characteristics, including wavelength-dependent apodization and phase errors of multichannel gratings should be understood and controlled, for an actual spectrometer to approximate its design performance. Aberration correction by the grating could also be used to advantage in controlling the performance variation across the field.

This work was done by Pantazis Mouroulis of Caltech for **NASA's Jet Propulsion Laboratory**. *Further information is contained in a TSP [see page 1].*

In accordance with Public Law 96-517, the contractor has elected to retain title to this invention. Inquiries concerning rights for its commercial use should be addressed to

Technology Reporting Office
JPL
Mail Stop 122-116
4800 Oak Grove Drive
Pasadena, CA 91109
(818) 354-2240

Refer to NPO-20343, volume and number of this NASA Tech Briefs *issue, and the page number.*

Mathematical Model of Vortex Pyrolysis of Biomass

Numerical simulations provide guidance for designing efficient reactors.

NASA's Jet Propulsion Laboratory, Pasadena, California

A mathematical model has been developed for analyzing the steady-state performances of vortex pyrolysis reactors used to convert particles of raw biomass materials (usually small wood chips) into char, tar, and gas. Optimal designs are usually considered to be those that maximize the production of tar. This model and its submodels can be regarded as more highly evolved versions of the model and submodels described in "Mathematical Model of a Direct-Contact Pyrolysis Reactor" (NPO-20069), page 62, "Mathematical Model of Pyrolysis of Biomass Particles" (NPO-20070), page 58, "Generalized Mathematical Model of Pyrolysis of Biomass" (NPO-20068), page 60, and "Production of Tar in Pyrolysis of Large Biomass Particles" (NPO-20067), page 83, *NASA Tech Briefs*, Vol. 22, No. 2 (February 1998).

Vortex reactors have been investigated for commercial production of tar from biomass because they are able of rapid heating of biomass particles through direct-contact ablation, and thereby offer the potential to achieve relatively high efficiencies. In a vortex reactor (see figure), the biomass particles are injected, along with a flow of a hot feed gas (usually, superheated steam), tangentially into a vertical cylindrical chamber with a heated wall. In the resulting strongly swirling flow of particles and gas, the particles are held against the wall by the centrifugal force.

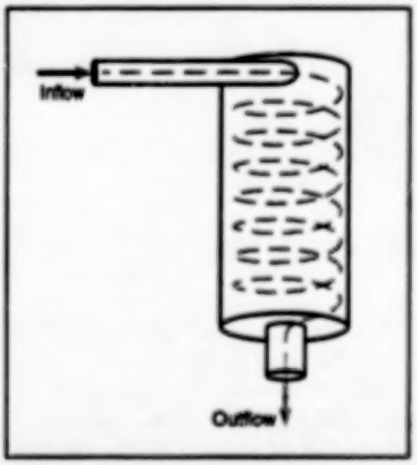

A Vortex Reactor features a strong swirling flow of gas and particles, with resultant direct-contact ablation and rapid heating.

Thus, the particles are heated primarily by direct conduction from the wall.

Pyrolysis causes layers of char to form on the particles. The char layers could retard pyrolysis because they are partially thermally insulating, but, as the particles continue to slide along the wall, they are scraped off (ablated). This ablation brings the unpyrolyzed remainders of the particles closer to the wall, thereby increasing the effective rates of heating and pyrolysis. Incompletely pyrolyzed particles that reach the outlet at the bottom of the reactor are collected and reinjected at the inlet along with the hot gas and the raw feedstock.

Like the previously reported model, the present mathematical model for the steady-state performance of the vortex reactor includes submodels of pyrolysis of particles, turbulent flow, and particle trajectories. The pyrolysis submodel is based on the one reported previously, with a modification to account for ablation by providing for fragmentation of char when the char attains a critical porosity. The flow submodel is one of compressible flow with a transport-equation sub-submodel of each component of the Reynolds stress tensor. In the particle-trajectory submodel, each particle is represented as moving under the combined influences of the flow (with drag forces represented by a simplified sub-submodel of flow in the immediate vicinity of the particle) and friction with the wall.

These submodels are coupled through boundary conditions and conservation laws, and the resulting equations of the overall model are solved numerically. The rates of injection of feedstocks and distribution of initial particle sizes are specified for steady-state operation. The distribution of particle sizes is altered as particles make repeated passes through the reactor, so that steady-state operation is characterized by, among other things, multiple particle-size distributions, each representing particles at a different stage of pyrolysis.

Numerical simulations that have been performed thus far with this model have yielded information pertinent to designing vortex pyrolysis reactors. In particu-

lar, a wall temperature of about 900 K was found to maximize tar yield; this temperature is practically independent of initial particle sizes. Analysis of the numerical results also revealed that a small reactor could not be scaled up successfully, so that it is recommended that pyrolysis at industrial scales (large mass feed rates) should be envisaged by using multiple small reactors operating in parallel rather than a single large reactor.

This work was done by Josette Bellan and Richard Miller of Caltech for **NASA's Jet Propulsion Laboratory**. *Further information is contained in a TSP [see page 1].*

NPO-20258

Highly Stable Lateral-Transfer Retroreflectors

Thermally induced beam deviations can be limited to the arc-second range.

Goddard Space Flight Center, Greenbelt, Maryland

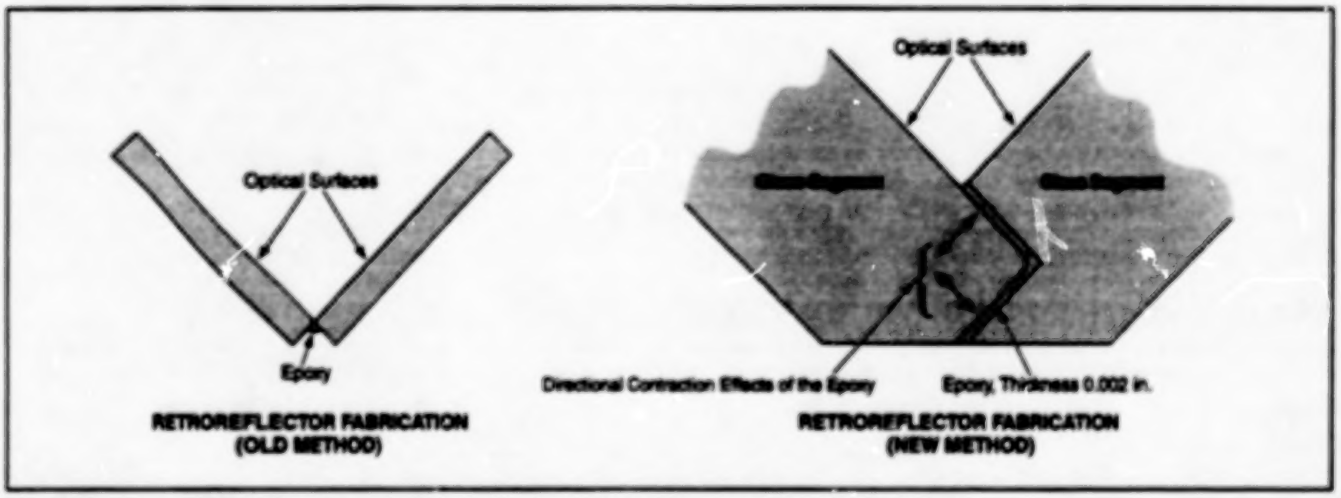

The Differences in Fabrication are compared here for the earlier and improved retroreflector designs.

Lateral-transfer optical retroreflectors can now be made extremely stable to both external and internal fluctuations and gradients of temperature. As explained in more detail in the fourth paragraph, this high stability is achieved through improvements in design and fabrication.

A lateral-transfer retroreflector is similar to the more familar corner-cube reflector in that (1) it includes three optically flat mirrors co-aligned and bonded in place so that each optical face is perpendicular to the other two faces and (2) by virtue of this mutual perpendicularity, regardless of its orientation, it always reflects a beam of light back along a line parallel to the direction of incidence. However, unlike in a corner-cube reflector, only two of the mirrors are adjacent. The third mirror is mounted out on an arm, away from the other two mirrors, so that the retroreflected light beam is displaced laterally from the incident light beam by a distance that depends on the length of the arm. Thus, a lateral-transfer retroreflector is useful for picking off a portion of a light beam and sending it back to a location laterally displaced from the source.

Heretofore, in the fabrication of a retroreflector, the usual practice has been to bond the mirrors together by use of epoxy along back seams as shown on the left side of the figure. When the retroreflector is then subjected to a temperature below the fabrication temperature, the epoxy shrinks, giving rise to tensile stresses on the backs of the mirrors. These stresses cause the mirrors to undergo angular misalignments that are small but nevertheless unacceptable because they give rise to degradation or loss of the retroreflective optical function.

In the improved design, the seams (where the faces are bonded) have a tongue-in-groove configuration, which makes it possible to put epoxy on two different surfaces in each seam. This configuration (depicted on the right side of the figure) causes the stresses engendered by cooling the retroreflector to below the fabrication temperature to become distributed across two planes perpendicular to each other. The result is a bond that does not allow change in either direction because the epoxy is essentially working against itself and unable to pull the mirrors out of alignment.

As part of a demonstration of this concept, a lateral-transfer retroreflector with a beam deviation of 11 arc seconds and a peak-to-valley wavefront error of 0.3 waves at a wavelength of 633 nm was constructed. The beam deviation was shown to change by less than 1 arc second when the retroreflector was subjected to an internal temperature gradient characterized by a temperature difference of 30 °C between the seam of the dihedral mirror subassembly and the mirror at the other end of the arm.

This work was done by James J. Lyons III of **Goddard Space Flight Center**. *No further documentation is available.*

GSC-14056

Books and Reports

Optical Diagnostics of High-Pressure Liquid Fuel Sprays

A report describes experiments in which nonintrusive optical diagnostic techniques were applied to high-pressure fuel sprays in simulated advanced turbine-engine combustor environments. The experiments involved three different fuel injectors in two unique optically accessible combustors: a radially-staged gas turbine combustor designed for testing multiple injectors and a flame tube designed for testing single injectors. Flows were observed at inlet temperatures from 533 to 810 K, inlet pressures from 0.55 to 1.7 MPa, and various mass flow rates. Planar laser-induced fluorescence and planar Mie scattering were used to image distributions of sprayed fuel, while phase Doppler particle analysis was performed to determine size and velocity distributions of fuel droplets. Analysis of the data thus acquired led to the conclusions that (1) differences among spray patterns for different fuel injectors and operating conditions are readily observable and (2) fuel-spray angles can easily be measured under realistic conditions. This work clearly demonstrates utility of these nonintrusive optical techniques for investigating fuel-spray patterns in realistic turbine-engine combustor environments.

This work was done by R. J. Locke of NYMA, Inc., and Y. R. Hicks, R. C. Anderson, and M. M. Zaller of **Lewis Research Center.** *To obtain a copy of the report, "Fuel Injector Pattern Evaluation in Advanced Liquid-Fueled, High-Pressure, Gas Turbine Combustors, Using Nonintrusive Optical Diagnostic Techniques," access the Technical Support see TSP's [page 1].*

Inquiries concerning rights for the commercial use of this invention should be addressed to NASA Lewis Research Center, Commercial Technology Office, Attn: Steve Fedor, Mail Stop 4–8, 21000 Brookpark Road, Cleveland, Ohio 44135. Refer to LEW-16701.

On the Validity of Using Assumed PDFs in Modeling Two-Phase Mixing

A report describes an investigation of the validity of using statistical methods based on single-point probability density functions (PDFs) in mathematical modeling of mixing between a turbulently flowing carrier gas and the vapor from liquid drops suspended in the gas. The investigation included theoretical analysis and comparisons with results of direct numerical simulations (DNS) of a two-phase mixing layer. Noting that Favre density-weighted averaging is the most convenient form for statistical-moment-transport equations for such flows, algebraic relations that illustrate the conditions under which PDFs can be determined accurately from Favre moments were derived. Comparisons with results of DNS showed that mixture-fraction Favre moments were nearly identical to the corresponding nonweighted moments. A transport equation for the Favre mixture-fraction variance that contains four new terms representing evaporation effects was then derived. Results of DNS indicated that one of these terms, due to scalar-source correlations, is predominantly responsible for production of scalar variance, while the other three terms are negligible. Finally, the β PDF, which represents well the DNS mixture-fraction statistics for single-phase mixing, was shown to be a poor representation for mixing of vapor from the droplets.

This work was done by Josette Bellan and Richard S. Miller of Caltech for **NASA's Jet Propulsion Laboratory.** *To obtain a copy of the report, "On the Validity of the Assumed PDF Method for Modeling Binary Mixing/Reaction of Evaporated Vapor in Gas/Liquid-Droplet Turbulent Shear Flow," see TSP's [page 1].*
NPO-20431

Properties of Ni/Zr Melts Related to Formability of Glasses

A report describes a study of the relationships between (1) the viscosities and specific volumes of Ni/Zr melts and (2) the formability of Ni/Zr-alloy metallic glasses. Experiments were performed on electrostatically levitated, radiantly heated molten specimens of two compound-forming and two eutectic Ni/Zr alloys, using noncontact diagnostic instrumentation. One of the findings from the experimental data was that the specific volume of the $NiZr_2$ alloy is significantly less than that of an ideal mixture of Ni and Zr, indicating the association of Ni and Zr in $NiZr_2$ molecules. Analysis of data revealed that the presence of $NiZr_2$ could account for observed configurational arrest above the melting temperature under a moderate cooling rate, and for observed small undercooling prior to crystallization. The viscosities of the compound-forming alloys were found to be larger than those of the eutectic alloys, indicating that the NiZr and $NiZr_2$ compounds are present. The viscosity data also indicated that these compounds are stable at temperatures above their melting points. It was concluded that a small specific volume or a large viscosity resulting from the presence of $NiZr_2$ or NiZr facilitates the formation of glass primarily by slowing the growth of crystalline phases.

This work was done by Won-Kyu Rhim, Kenichi Ohsaka, and Sang K. Chung of Caltech for **NASA's Jet Propulsion Laboratory.** *To obtain a copy of the report, "The specific volumes and viscosities of the Ni-Zr liquid alloys and their correlation with the glass formability of the alloys," see TSP's [page 1].*
NPO-20368

BLANK PAGE

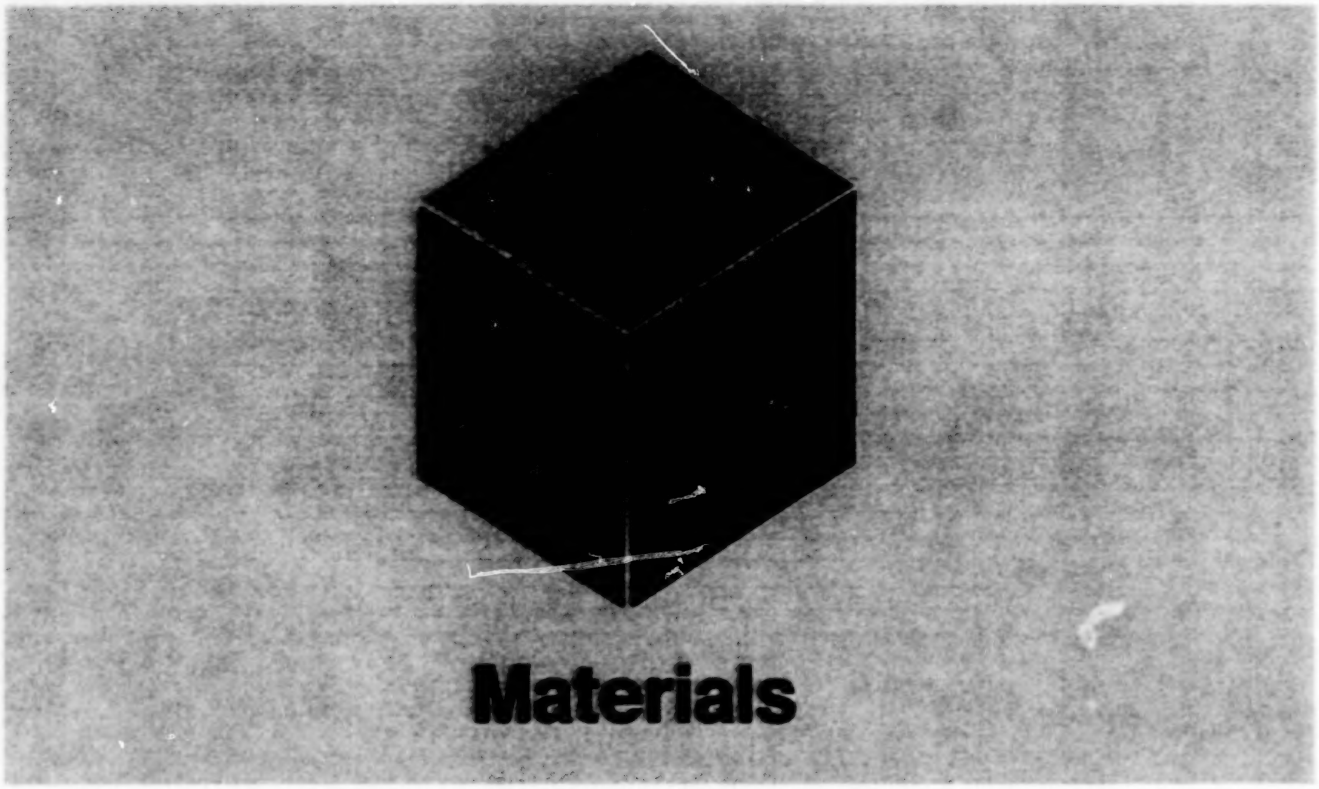

Materials

Hardware, Techniques, and Processes

BLANK PAGE

Room-Temperature, Ultraviolet Curing of Polyimides

Diels-Alder reactions are used to trap unstable intermediate compounds.

Lewis Research Center, Cleveland, Ohio

Polyimides have been used widely in fiber-reinforced composite materials for aerospace components and in thin films for packaging of electronic circuitry. Typically, the synthesis of a material of this type involves the condensation of a diamine with a dianhydride. This synthesis also produces low-molecular-weight byproducts, e.g., water, which can cause problems in processing the polyimide that one seeks to

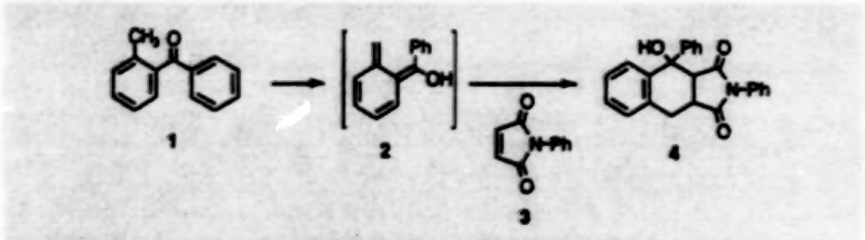

Figure 1. A Photoenol (compound 2) is generated from *o*-methylbenzophenone (compound 1), then trapped by use of a maleimide (compound 3), yielding compound 4.

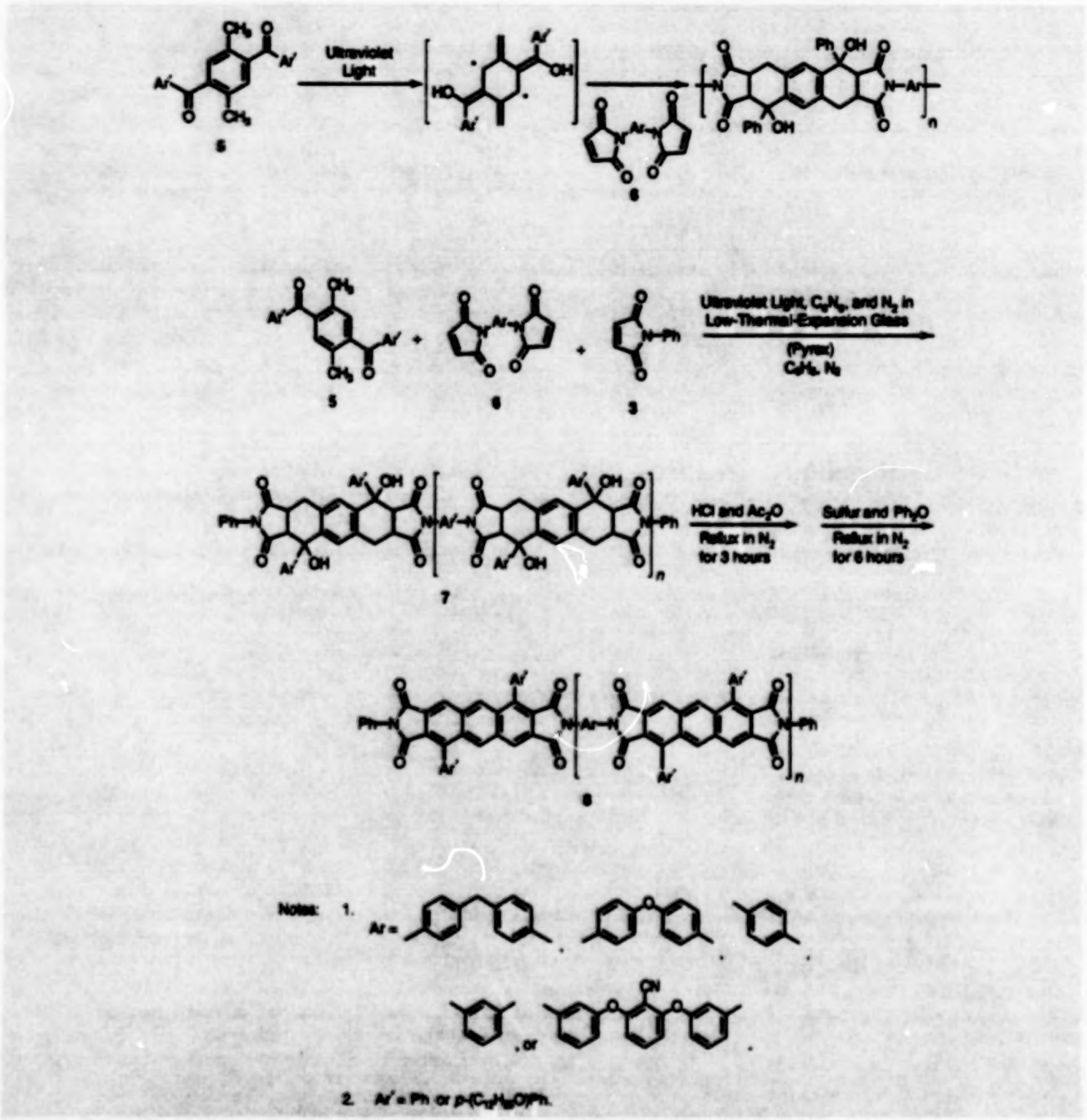

Figure 2. Polyimides Are Produced via Diels-Alder trapping of photochemically generated bisdienes.

produce. In addition, health concerns about the handling of aromatic diamines — which are often toxic, mutagenic, or carcinogenic — give rise to requirements to use costly engineering controls in the workplace to limit exposure to these compounds.

Over the years, other approaches to the synthesis of polyimides have been developed to address these problems and concerns. Diels-Alder polymerizations — usually involving a bismaleimide and a stable bisdiene, such as a bisfuran — have been investigated extensively. More recent work in this area has focused on the use of reactive diene intermediates, such as *o*-quinodimethanes generated from benzocyclobutenes. To date, most if not all of these approaches have entailed the use of high reaction temperatures (above 200 °C).

A new Diels-Alder route to the synthesis of polyimides involves the use of ultraviolet light, rather than heat, to effect polymerization. This approach is based upon a well-known class of photochemical reactions — the photoenolization of *o*-methylphenyl ketones — which can be carried out at room temperature. For example (see Figure 1) the irradiation of an *o*-methylphenyl ketone (compound 1) with ultraviolet light of wavelengths above 300 nm produces a photoenol (compound 2). This photoenol is unstable, but persists long enough to undergo Diels-Alder reactions with typical dienophiles, such as a maleimide (compound 3).

By utilizing a diketone, such as 2,5-dibenzoyl-*p*-xylene (compound 5) and a bismaleimide (compound 6), this chemistry can be used to make polyimides (see Figure 2). A number of polyimides (represented as compound 7), have been prepared by following this approach. Glass-transition temperatures for these polyimides can be as high as 300 °C. These polyimides exhibit modest stabilities in both air and nitrogen. Temperatures of onset of decomposition, measured by thermal gravimetric analysis (TGA), are as high as 400 °C in air and 450 °C in nitrogen. Higher glass-transition temperatures and temperatures of onset of decomposition can be obtained by conversion of compound 7 into compound 8 through acid-catalyzed dehydration followed by dehydrogenation. Polyimides represented as compound 8 have glass-transition temperatures as high as 330 °C and temperatures of onset of decomposition as high as 550 °C in air and 525 °C in nitrogen.

This chemistry has been demonstrated in solution (benzene or cyclohexanone), but should be easily adaptable to achieve solid-state (solvent-free) curing. Such adaptation would make the present approach particularly suitable for thin-film applications (e.g., coatings, electronics packaging, and photonic/optical materials). This ultraviolet-curing approach could offer several advantages over other approaches to the preparation of polyimides. Ultraviolet-cured films should undergo less shrinkage during cure than do those films that are cured at high temperatures. This approach would be useful for the curing of polyimides that contain such thermally sensitive groups or additives as nonlinear optical materials. In addition, this approach does not entail some of the disadvantages of condensation-chemistry-based approaches; namely, the formation of volatiles during cure, health risks associated with the use of diamines, and poor solution stability.

This work was done by Michael A. Meador and Mary Ann B. Meador of **Lewis Research Center**, *Lesley L. Williams of Spelman College, and Jeremy R. Jones of NASA Center for High Performance Polymers and Composites, Clark Atlanta University. Further information is contained in a TSP [see page 1].*

Inquiries concerning rights for the commercial use of this invention should be addressed to NASA Lewis Research Center, Commercial Technology Office, Attn: Tech Brief Patent Status, Mail Stop 7–3, 21000 Brookpark Road, Cleveland, Ohio 44135. Refer to LEW-16568.

Improved Synthesis of SnO Powder for Lithium-Ion Power Cells

This powder gives better electrochemical performance and costs less.

NASA's Jet Propulsion Laboratory, Pasadena, California

An improved method of synthesis of crystalline tin monoxide (SnO) powder for use in anodes of lithium-ion electrochemical power cells has been developed. The carbon used in anodes of Li-ion cells is relatively expensive and difficult to produce, and SnO has been found potentially useful as an alternative anode material. One major disadvantage of the method heretofore followed in producing commercial crystalline SnO powder is that it involves heating. The improved method does not involve heating and thus offers the potential to reduce the cost, time, consumption of energy, and risk of contamination in the production of crystalline SnO powder. Fortuitously, it turns out that the improved method also yields powder with greater specific surface area, making it possible to fabricate electrodes with reversible charge/discharge capacities, for a fixed rate, greater than those of electrodes made from commercial crystalline SnO powder.

In the commercial method, synthesis begins with the dissolution of metal-ion-containing salt in distilled water. The resulting solution is added dropwise into a basic (e.g., NaOH) solution, where, typically, particles of amorphous metal hydroxide precipitate. The precipitate particles are washed, filtered, and dried in air. Next, the precipitate particles are heated in a crucible in air to a temperature typically above 200 °C to transform them from amorphous metal hydroxide to crystalline tin monoxide.

The improved method is derived from the commercial method but differs in key respects. Instead of starting by completely dissolving metal-ion-containing salt, one starts with an insoluble combination of $SnCl_2$ in water to form $Sn_xO_yH_z$ compounds. The tin-bearing solution obtained by hydrolysis in the improved method is acidic. The tin-bearing acidic solution is added dropwise to a basic solution (NaOH or NH_4OH). However, whereas the pH of the basic solution is allowed to fall to about 10 or 11 as the acidic solution is added dropwise in the commercial method, the pH is not allowed to fall in the improved method; instead, NaOH is added continuously to maintain the pH of the basic solution at 14 during the dropwise addition of the acidic tin-bearing solution. A white gel precipitate is formed and, after about 45 minutes, becomes transformed into a black precipitate comprising aggregated crystalline SnO powder. The precipitate is washed, filtered, and dried as in the commercial method, but unlike in the commercial method, no further processing (that is, no heating) is needed.

The electrochemical performance of crystalline SnO powder synthesized by the commercial method (SnO-COM) and of SnO powder synthesized by the improved method with no heating (SnO-NH) were measured during charging and discharging of half cells. Each half cell included a

nickel-mesh-supported lithium foil that served as both an anode and a reference electrode, plus a cathode fabricated by spraying a mixture of SnO powder, a poly(vinylidene fluoride) binder, and carbon black onto a copper foil substrate. The electrodes in each cell were separated by 50-μm-thick polypropylene membranes. The cells were filled with an electrolyte mixture of $LiPF_6$, ethylene carbonate, and dimethyl carbonate.

The figure presents titration curves from charging and discharging of the half cells between a charge cutoff potential of 1.2 V and a discharge cutoff potential of 0 V. These curves indicate a greater specific charge capacity for the SnO-NH electrode than for the SnO-COM electrode. The increase in specific capacity can be attributed to greater specific surface area (0.871 m^2/g for SnO-NH vs. 0.297 m^2/g for SnO-COM). This effect increases the accessible electrode surface area and ease of incorporation and extraction of Li ions.

This work was done by Chen-Kuo Huang and Subbarao Surampudi of Caltech and Jeffrey Sakamoto and Jeffrey Wolfenstine of UC Irvine for **NASA's Jet Propulsion Laboratory.** *Further information is contained in a TSP [see page 1].*
NPO-20355

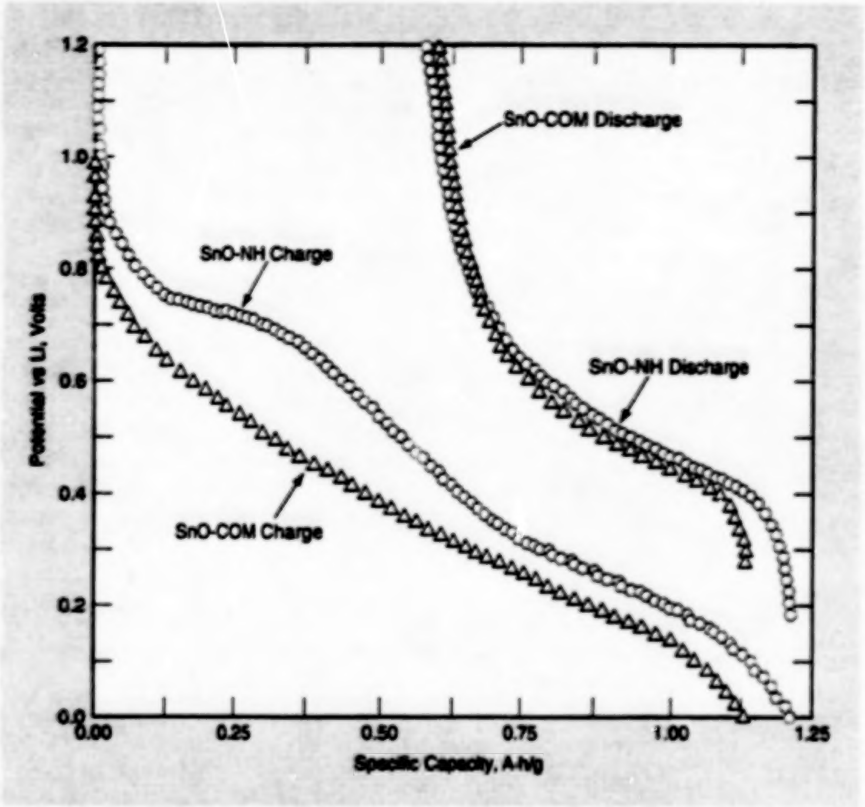

These Titration Curves from charging and discharging of Li/SnO half cells have been interpreted as signifying that the initial reversible capacity of the electrode made with SnO-NH was about 20 percent greater than that of the electrode made with SnO-COM.

Reaction-Forming Method for Joining SiC-Based Ceramic Parts

Joints can be formed with tailorable thicknesses, compositions, and thermomechanical properties.

Lewis Research Center, Cleveland, Ohio

Reaction-Formed Joints of Different Thicknesses between samples of reaction-bonded SiC exhibited different microstructures, compositions, and mechanical properties.

A process that involves reaction bonding makes it possible to form strong joints, with tailorable thicknesses and compositions, between high-temperature-resistant structural parts made of SiC-based ceramic materials. These parts and materials are being developed for use as engine components, radiant-heater tubes, heat exchangers, components of fusion reactors, furnace linings, furnace bricks, and components for diffusion processing in the microelectronics industry. The process can be used to join simply shaped parts to make complexly shaped structures, and to repair such parts and structures.

The present process is a successor to the process reported in "Joining of SiC-Based Ceramic and Fiber-Reinforced Composite Parts" (LEW-16405), *NASA Tech Briefs*, Vol. 22, No. 5 (May 1998), page 54. The process begins with the application of a carbonaceous mixture (typically in paste form) to the joint regions between parts, immediately followed by clamping of the parts in a fixture. The thickness of the joint can be tailored by choice of the properties of the

carbonaceous mixture and of the clamping force. The carbonaceous mixture is cured at a temperature between 110 and 120 °C for 10 to 20 minutes. The curing step fastens the parts together (albeit not yet at full strength), making it unnecessary to fabricate a special fixture to hold the parts together during subsequent high-temperature processing.

After curing of the carbonaceous layer, silicon or a silicon alloy in tape, paste, or slurry form is applied to the joint region. Then the parts are heated to a temperature between 1,250 and 1,425 °C for 5 to 10 minutes, the precise temperature and time depending on the applied material. The heating causes the silicon to melt, infiltrate the joint, and react with carbon. As a result, the finished joint contains silicon carbide with amounts of silicon and other phases that can be tailored by choice of the compositions of the reactants. Consequently, the process results in joints with tailorable microstructures and thus tailorable thermomechanical properties. The properties of the joints can thus be tailored to approximate closely those of the joined parts.

The figure depicts the microstructures of selected experimental reaction-formed joints of three different thicknesses between samples of a commercially available reaction-bonded silicon carbide. The thickest of these joints was found to consist mainly of Si with small amounts of SiC, and to be susceptible to brittle fracture. The thinnest of these joints were found to consist of SiC and Si phases. At both room temperature and temperatures up to 1,350 °C in air, the strength of the material in the thinnest joints was found to be at least equal to and, in some cases, greater than, that of the adjacent SiC sample materials.

This work was done by M. Singh of NYMA, Inc., for **Lewis Research Center.** *Further information is contained in a TSP [see page 1].*

Inquiries concerning rights for the commercial use of this invention should be addressed to NASA Lewis Research Center, Commercial Technology Office, Attn: Tech Brief Patent Status, Mail Stop 7–3, 21000 Brookpark Road, Cleveland, Ohio 44135. Refer to LEW-16661.

Diffusing Hf and Si Into Aluminide Bond Coats for TBCs

Turbines could be operated at higher temperatures.

Lewis Research Center, Cleveland, Ohio

A process for making superior diffusion platinum-aluminide bond coats for plasma-sprayed or physical-vapor-deposited thermal-barrier coats (TBCs) on superalloy substrates has been devised. The novel aspect of the process lies in the use of several relatively inexpensive pack diffusion steps to incorporate hafnium and silicon to increase resistance to oxidation.

TBCs are typically composed of yttria-stabilized zirconia and are typically used to protect superalloy turbine-engine components against high temperatures. A bond coat provides both mechanical and chemical bonding between the underlying superalloy and the overlying TBC. Diffusion-type aluminide bond coats offer advantages (including lower cost) over conventional MCrAlY (where "M" denotes Fe or Ni) bond coats, except that the diffusion-type aluminide coats exhibit lower resistance to oxidation. Any change in material or processing that increases the ability of bond coats to resist oxidation also increases the durability of TBC coats.

The incorporation of Pt into a diffusion-type aluminide bond coat increases its resistance to oxidation. Prior to the development of the present process, Hf and Si had been incorporated into MCrAlY bond coats to increase resistance to oxidation, but had not been incorporated into diffusion Pt-aluminides.

The basic version of the present process comprises the following steps:

1. A hafnided surface layer with a thickness between 0.5 and 1 mil (between 13 and 25 μm) is formed on a superalloy substrate by pack diffusion of Hf at a temperature of 1,975 °F (1,079 °C) for 4 hours.
2. A thin surface layer of Si is deposited by pack siliciding.
3. The hafnided, silicided workpiece is plated with Pt to a thickness between 0.2 and 0.3 mils (between 5 and 8 μm).
4. The workpiece is diffusion heat-treated at a temperature of 1,900 °F (1,038 °C) for 2 hours.
5. The workpiece is vapor-phase or pack aluminized.
6. The workpiece is given a post-aluminiding heat treatment to homogenize the coating.

The superior bond coats afforded by this process enable affected turbine components to withstand higher operating temperatures; higher operating temperatures result in greater energy-conversion efficiencies. Moreover, the superior bond coats provide some residual protection for parts from which TBCs have spalled.

This work was done by Bhupendra K. Gupta and Jon C. Schaeffer of General Electric Co. for **Lewis Research Center.** *Further information is contained in a TSP [see page 1].*

Inquiries concerning rights for the commercial use of this invention should be addressed to NASA Lewis Research Center, Commercial Technology Office, Attn: Tech Brief Patent Status, Mail Stop 7–3, 21000 Brookpark Road, Cleveland, Ohio 44135. Refer to LEW-16295.

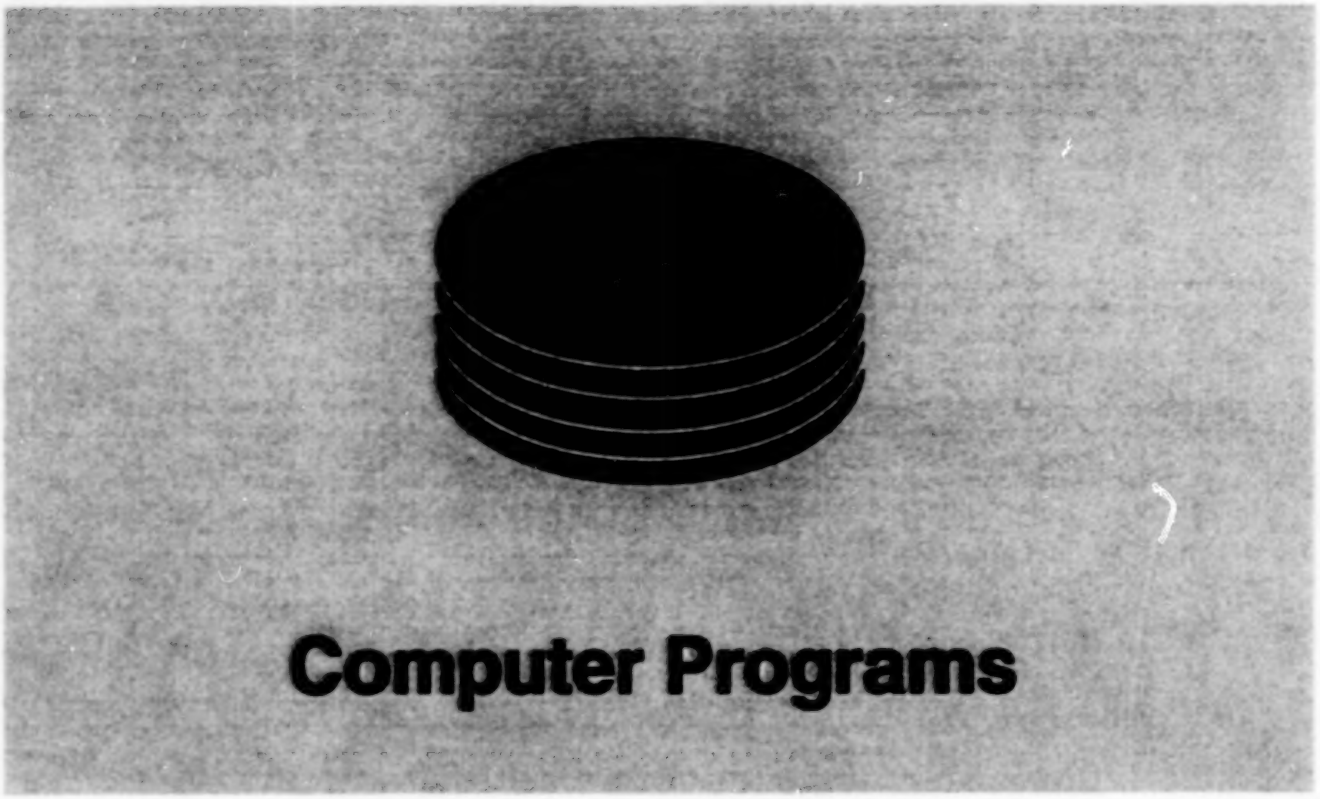

Computer Programs

BLANK PAGE

Computer Programs

These programs may be obtained from COSMIC. Please contact

COSMIC®
Computer Services Annex
University of Georgia
Athens, GA 30602
Telephone No. (404) 542-3265.

Physical Sciences

Software Detects Small Satellites in Spacecraft Imagery

A computer program processes images acquired at different times by instrumentation aboard a spacecraft to detect small satellites of asteroids and other planetary bodies. The program coregisters the images, removes instrument artifacts and images of background stars, and performs a thresholding operation to suppress noise and generate binary version of the images. The program then searches the binary images for persistent objects, which when found, are put on a list of candidate satellites. The entire process takes place automatically, without human intervention. The data on the candidate satellites can be sent to an autonomous spacecraft executive program for targeting of the spacecraft and/or its instrumentation. The program may also be adaptable to terrestrial use in automated detection of objects and avoidance of hazards. At present, the program runs under Matlab on Sun workstations running Solaris. Plans call for a final version in C under the VxWorks operating system in a RAD6000 processor.

This program was written by Paul Stolorz, Victoria Gor, and Richard Doyle of Caltech and Clark Chapman, Randy Gladstone, William Merline, and Alan Stern of the Southwest Research Institute for **NASA's Jet Propulsion Laboratory**. *For further information, see TSP's [page 1].*
NPO-20201

Mathematics and Information Sciences

Easy-to-Use Software for Planning and Scheduling

The Automated Planning and Scheduling Environment (ASPEN) version 2 computer program comprises a modular, reconfigurable software framework and collection of software components that can be used for automated planning and scheduling in a variety of applications. ASPEN can automatically generate schedules pursuant to high-level goals specified by the user. ASPEN can also provide automated assistance, with human intervention, in the correction of previously generated faulty schedules. The primary advantages of ASPEN are simplicity and ease of use. Features include a heuristic specification language to provide guidance for the automatic-scheduling software components, an external function interface that facilitates integration with other software, and a graphical user interface for viewing and manipulating schedules. ASPEN was written in C++ for execution on a Sun Workstation running Solaris 2.5-2.6 with at least 32MB of random-access memory and 1GB of disk storage. The Objectspace STL Library and Java Runtime Environment are necessary for execution. The graphical user interface (GUI) can also be run on a PC with the Java Runtime Environment.

This work was done by Robert Sherwood, Steve Chien, Gregg Rabideau, Anita Govindjee, Alex Fukunaga, David Yan, and Russell Knight of Caltech for **NASA's Jet Propulsion Laboratory**. *For further information, see TSP's [page 1].*
NPO-20299

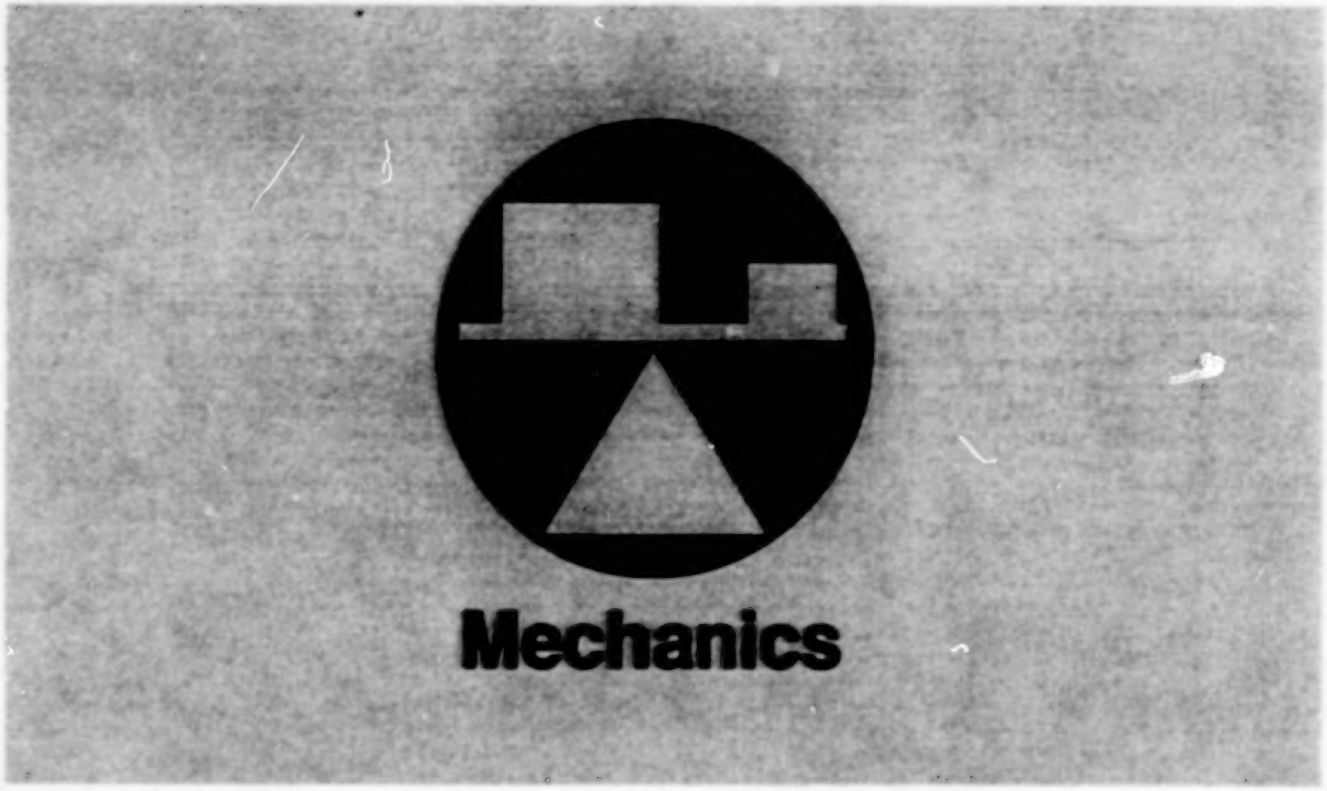

Hardware, Techniques, and Processes

BLANK PAGE

Stable, Soft-Opening/Soft-Closing Pressure-Relief Valves

The risk of ignition in systems containing oxygen is reduced.

Stennis Space Center, Mississippi

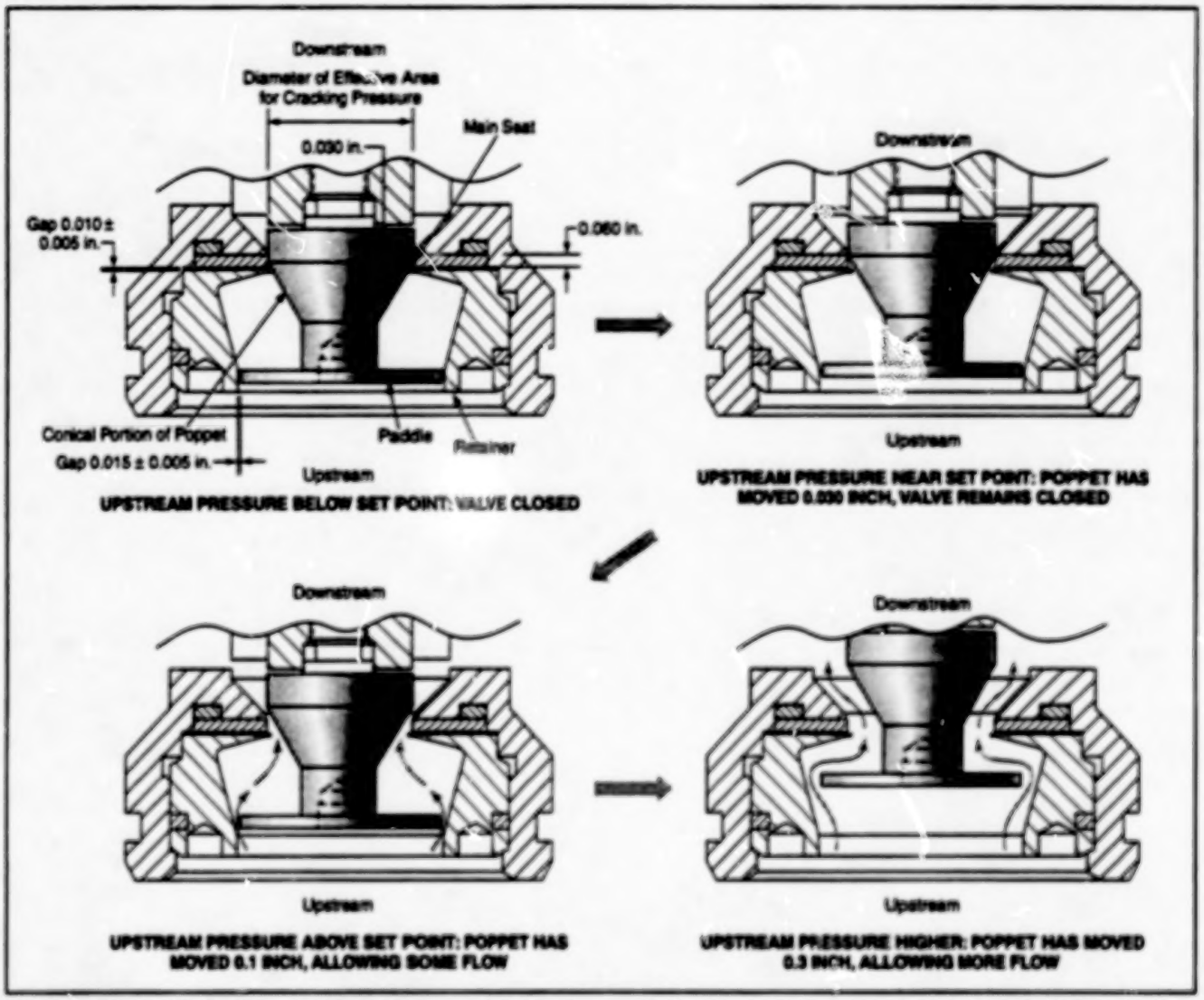

This Valve Operates Under Upstream Control in the sense that the flow-constricting cross section is the annulus between the paddle and retainer, upstream from the annulus between the poppet cone and the main valve seat. The few dimensions shown here are typical only; the dimensions for a specific application are chosen, with the help of a mathematical model of valve dynamics, to obtain stable operation.

Improved pressure-relief valves have been developed for systems that contain gases and liquids in a variety of pneumatic, hydraulic, and cryogenic applications. These valves could prove especially beneficial in both cryogenic and non-cryogenic systems that contain oxygen. The improved valves are designed to suppress instabilities that shorten operational lifetimes and create hazards in the operation of older pressure-relief valves.

A typical older pressure-relief valve exhibits instability that can result in oscillation ("chatter"), which degrades the valve beyond the normal anticipated wear of parts. Oscillation can result in hard impact; in the presence of oxygen, hard impact can lead to ignition, with resultant catastrophic failure of the valve and possibly of the entire system. A valve of the present improved type is stable over its entire operational range from fully closed to fully open. It does not oscillate or generate hard impacts; instead, it opens and closes softly.

The key to stable, soft-opening/soft-closing operation is a concept of upstream control. A conventional "pop"-type pressure-relief valve is characterized as operating under downstream control: Once the valve has opened, the flow is controlled mainly by an effective cross-sectional area downstream of the valve seat. In a valve of the improved type, the flow-limiting cross section remains upstream of the valve seat at all times, and so the valve is said to operate under upstream control.

The figure illustrates the basic design and principle of operation of a valve of the improved type. As in a conventional relief valve, excessive upstream pressure opens the valve by lifting of a poppet from a seat in a valve body; however, the similarity with a conventional pressure-relief valve ends here. The poppet in the improved valve includes a conical portion and a paddle (essentially a disk) upstream of the conical portion. When the valve is closed and the upstream pressure is below the set point, the conical portion of the poppet engages about half the thickness of a main valve seat, forming a tight seal. In this condition,

the paddle engages the wall of a cylindrical passage upstream of the main valve seat.

When the upstream pressure rises to approximately the set point, the poppet moves downstream a little, but the valve is not yet open, the conical portion of the poppet remains partly engaged with the main valve seat, while the paddle remains in the cylindrical passage in the retainer. As the pressure rises above the set point, the conical portion of the poppet moves out of the main valve seat and the paddle moves out of the cylindrical passage in the retainer. To ensure upstream control, the area of the annular opening between the main seat and the conical poppet surface must be made larger than the area of the annular opening between the paddle and the retainer; for this purpose, the angle of the conical inner valve-body surface immediately downstream of the main valve seat must be made greater than the angle of the conical inner valve-body surface immediately downstream of the cylindrical passage in the retainer.

The advantages of upstream control are:

- There are no adjustments other than the set point;
- There is a smooth transition from the fully closed to the fully open valve condition because there is minimal variation in density of fluid over a wide range of flow, and
- The upstream-control concept is amenable to mathematical modeling because the basic valve geometry (except for specific dimensions) is fixed. A user-friendly computer program based on a mathematical model of the valve dynamics can be used to design and select valves of this type for specific applications.

The improved valves offer several advantages over older pressure-relief valves, in addition to those mentioned above. Noise and wear are reduced through elimination of chatter. The risk of fire and explosion is reduced through elimination of hard impact, and the risk of uncontrolled venting of hazardous fluids is correspondingly reduced. Increased stability yields better performance, with wider operating ranges and better control. The basic valve design can be implemented in cartridge versions, so that it becomes unnecessary to remove entire valves from plumbing systems for overhaul or repair. The foregoing advantages translate to the additional advantage of lower life-cycle costs.

This work was done by Peter A. Tartaglia, Brian L. Magnone, Larry Rayhon, and Richard Molesworth of Marotta Scientific Corp. for **Stennis Space Center**.

In accordance with Public Law 96-517, the contractor has elected to retain title to this invention. Inquiries concerning rights for its commercial use should be addressed to

Peter Tartaglia
Marotta Scientific Controls Inc.
PO Box 427
Montville, NJ 07045
(973)334-7800 ext. 464

Refer to SSC-00073, volume and number of this NASA Tech Briefs issue, and the page number.

Push/Pull Four-Point-Bending Apparatus

Applied bending stress can be reversed during a test.

Goddard Space Flight Center, Greenbelt, Maryland

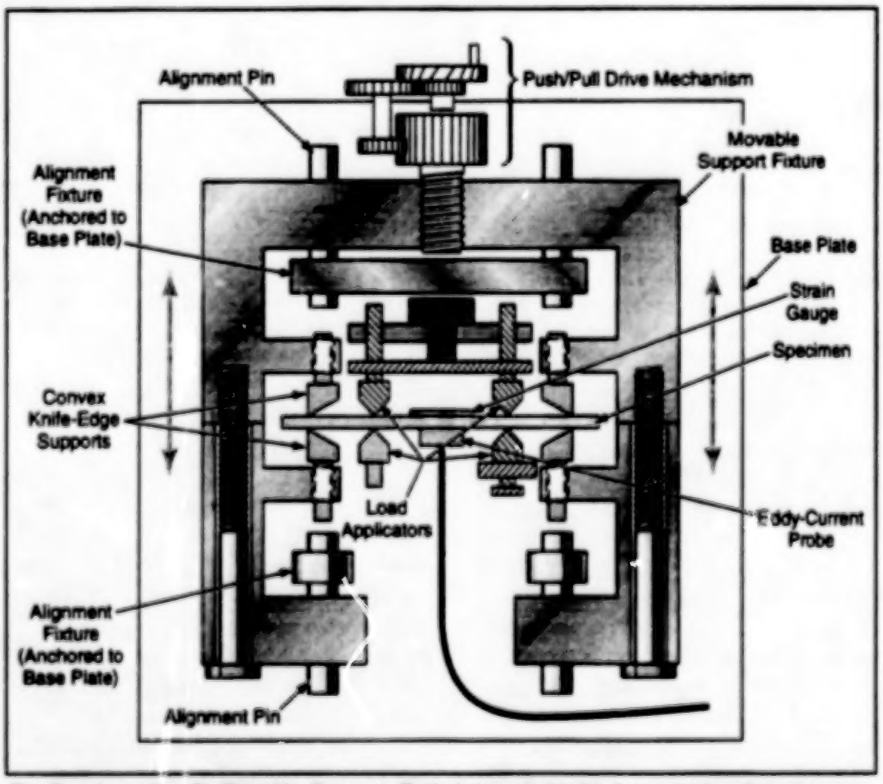

The Specimen Can Be Bent Up, Down, or Both during a test in this four-point bending apparatus.

The figure depicts an improved apparatus for three- or four-point bending tests of stripe specimens. In a bending test, the specimen is subjected to tension along its top surface and compression along its bottom surface, or vice versa. A three- or four-point bending fixture of older design is capable of pushing from one side only, so that it can bend the specimen in one direction only; that is, it can induce either tension or compression (but not both) on the top or bottom surface. The present apparatus is capable of pushing on a specimen from either side and thus bending the specimen in either direction. Thus, for example, the apparatus can be used to perform a test in which the applied stress is varied continuously from a maximum tension through zero to a maximum compression.

The specimen is placed between two pairs (for a four-point test) or one pair (for a three-point test) of knife-edge load applicators that are anchored on a base plate. One load applicator is fixed; the other three are adjustable. Pairs of convex knife-edge supports on a movable support fixture are also positioned in gentle contact (while in the zero-applied-stress condition) with the specimen near the ends of the specimen.

A manual push/pull drive mechanism translates the movable support fixture up or down to exert a compressive or tensile stress on the upper or lower surface of the specimen. Alignment pins ensure that the stress is applied perpendicularly to the nominal longitudinal axis of the specimen.

A strain gauge is attached to one side of the specimen and an eddy-current probe (or other sensor) to the other side. During the bending test, the eddy-current signal is recorded as a function of the strain. The eddy-current signal as a function of stress and/or strain yields information on residual stress in the specimen. Optionally, the apparatus could be automated by motorizing the drive mechanism and using the output of the strain gauge as a feedback control signal for the motor.

This work was done by E. James Chern of **Goddard Space Flight Center**. *No further documentation is available.*
GSC-13801

Noise-Reducing Fairings for Flush-Mounted Microphones

Noise is minimized by designs that favor laminar over turbulent flow.

Ames Research Center, Moffett Field, California

Streamlined fairings have been invented for housing single or multiple microphones to measure noise in flowing gases and liquids. Each fairing of this type is designed to minimize the spurious (background) component of noise generated by local flow disturbances caused by the fairing itself. These fairings could be used in measuring noise associated with a variety of flow sources, including aircraft, wind tunnels, air-handling equipment, and land vehicles.

The figure presents a cross section of a representative fairing of the present type. The microphones are mounted flush with the outer fairing surfaces to minimize acoustic distortion; in fairings invented previously for the same purpose, the microphones are typically mounted within recesses or cavities, the acoustic resonances of which distort the desired acoustic signals. Also, unlike some previously invented fairings, the microphones are not mounted behind porous screens that attenuate the desired acoustic signals. The outputs of the microphones are communicated to measuring or recording equipment via electrical or fiber-optic cables, or by telemetry.

To minimize the local flow disturbances that generate background noise, a fairing of this type is designed to obtain laminar flow under the widest practical range of anticipated flow conditions. In the example illustrated in the figure, the shape of the fairing and its orientation with respect to the flow are chosen to obtain an extended upstream surface with a favorable pressure gradient (pressure on the fairing surface decreasing with distance from the leading edge). The flow in a favorable pressure gradient tends to be naturally smooth or laminar over a wide range of speed; consequently, microphones placed in this region are exposed to minimum noise from local flow disturbances.

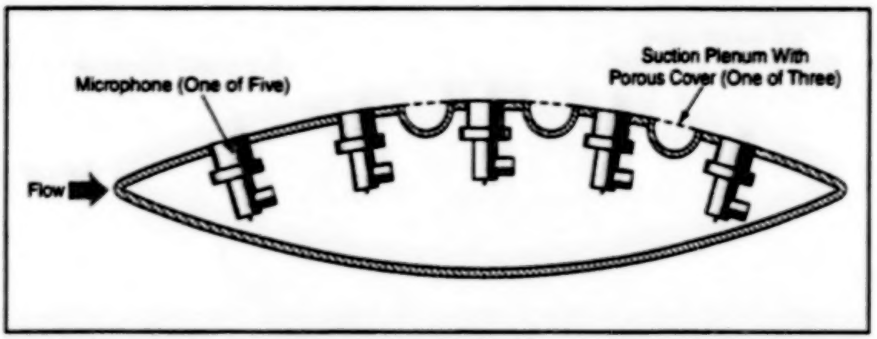

A conceptual illustration shows Sensor Fairing with five flush-mounted microphones with natural laminar flow upstream of the point of maximum thickness, and suction flow control to delay the onset of unsteady separation downstream of the point of maximum thickness. Suction flow control may also be used to maintain laminar flow to higher velocities and free-stream turbulence levels. In recent tests, natural laminar flow was maintained on the forward section of a fairing with 8 in. (0.2 m) chord to speeds of 100 kn (51.4 m/s) with free-stream turbulence level of 0.25 percent.

Above a critical speed that depends on the roughness of the fairing surface and the disturbance content of the free-stream flow, the flow along the upstream surface undergoes a transition from laminar to turbulent. The transition speed can be increased by cooling and/or by suction through small holes, slots, or porous surfaces; this phenomenon is well known in the aircraft industry and has been exploited to reduce drag on aerodynamic surfaces. Here, suction is applied to maintain laminar flow at speeds that would otherwise exceed the transition speed.

The pressure along the fairing surface downstream of the point of maximum thickness is increasing with downstream distance. The flow in this adverse pressure-gradient region tends to be turbulent at most speeds of interest, and the flow may separate from the fairing. Unsteady separation may cause an increase in drag and levels of self-noise. Suction control may also be used to delay the onset of flow separation at the trailing edge.

This work was done by William Clifton Horne and Kevin D. James of **Ames Research Center**. *Further information is contained in a TSP [see page 1].*

Inquiries concerning rights for the commercial use of this invention should be addressed to the Patent Counsel, Ames Research Center [see page 1]. Refer to ARC-14241.

BLANK PAGE

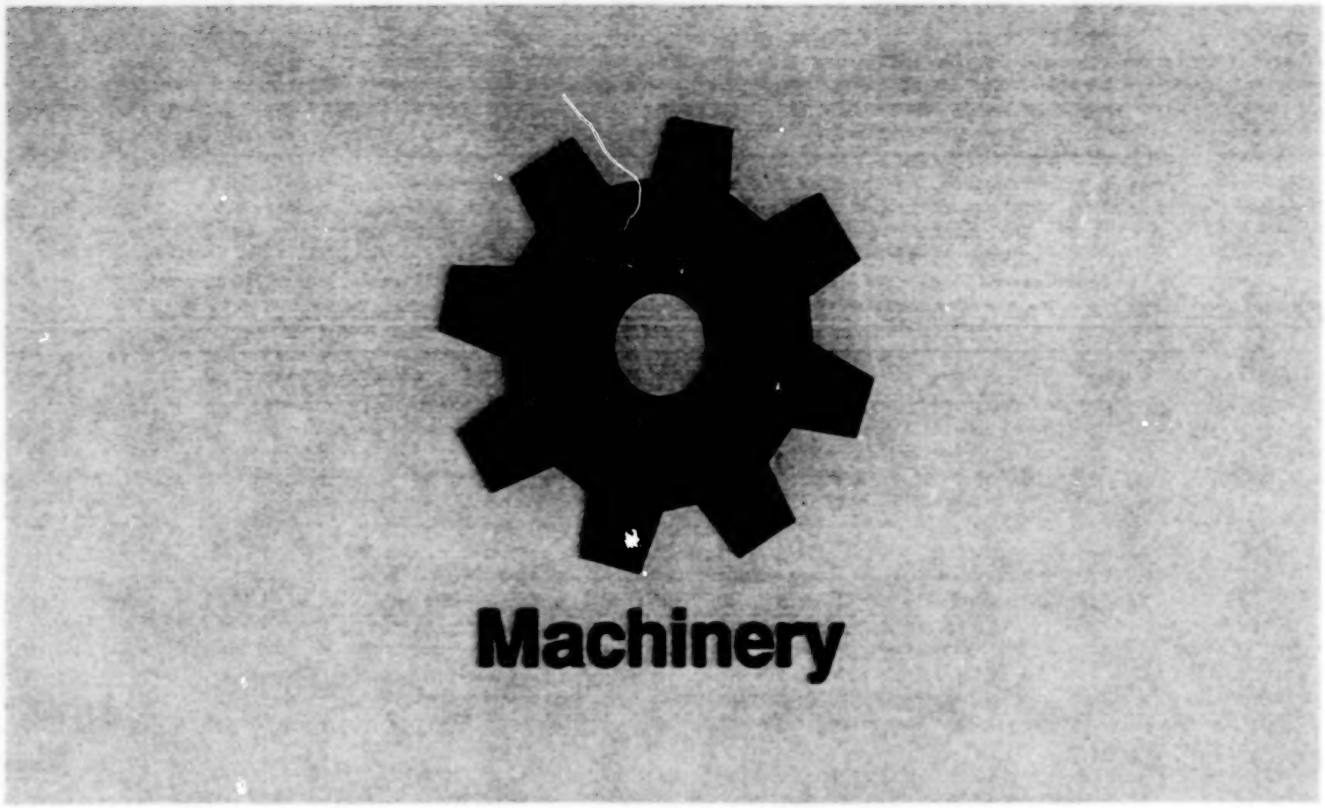

Machinery

Hardware, Techniques, and Processes

BLANK PAGE

Engines for Remotely Piloted Atmospheric-Science Airplanes

A reciprocating engine is a better answer in high-flight altitude.

Dryden Flight Research Center, Edwards, California

A Triply Turbocharged ROTAX Engine is currently regarded as the best choice for remotely piloted atmospheric-science airplanes.

A spark-ignited reciprocating gasoline engine, intake-pressurized with three cascaded stages of turbocharging, was selected by NASA's Environmental Research Aircraft and Sensor Technology (ERAST) Program, managed at the Dryden Flight Research Center, to propel the next generation of remotely piloted atmospheric-science airplanes. Scientific needs for sampling the atmosphere, and providing unique images of the Earth, dictate the unique required flight regime; namely, subsonic speeds at altitudes >80 kft (>24 km) and for periods exceeding 24 hours.

The unique nature of the sampling mission, coupled with the economics of engine development, point to the turbocharged, spark-ignited reciprocating engine (see figure) as the only cost-effective option. The table shows the subtle physical advantages of the reciprocating engine over the turbojet for high-altitude, low-speed flight, arising from its near-stoichiometric combustion. Its low specific air consumption reduces the amount and weight of turbomachinery

TURBOJET VERSUS TURBOCHARGED INTERNAL COMBUSTION ENGINE

Powerplant/Propulsion System (Inlet Recovery = 1.0)	Uninstalled Weight Incl. Propeller	Delivered Thrust	Specific Weight	Specific Consumption

Subtle Physical Advantages of the reciprocating engine are shown here over the turbojet for high-altitude, low-speed flights.

required to generate power at >80 kft, which apparently results in lower weight and lower thrust specific fuel consumption than a turbojet in this flight regime, despite the large heat exchangers.

The turbocharged engine is low cost because of the existing technology base of mass-produced automotive and general aviation hardware that can be adapted to build such an engine. In addition, the turbocharged engine is technically competitive with the turbine engine at high altitudes. Although the power density of a turbine engine is higher than the reciprocating engine at normal altitudes, the reciprocating engine begins to compare favorably with turbine engines at altitudes above 80 kft, especially at the lower speeds where inlet precompression is not available.

This work was done by James L. Harp, Jr., of ThermoMechanical Systems, Inc., with contributions from NASA Lewis Research Center for **Dryden Flight Research Center**. *To obtain a copy of the paper, "Propulsion System for Very High Altitude Subsonic Unmanned Aircraft," see TSP's [page 1].*

Inquiries concerning rights for its commercial use should be addressed to:

ThermoMechanical Systems, Inc.
20944 Sherman Way #210
Canoga Park, CA 91303
(818)884-9800

Refer to DRC-98-61.

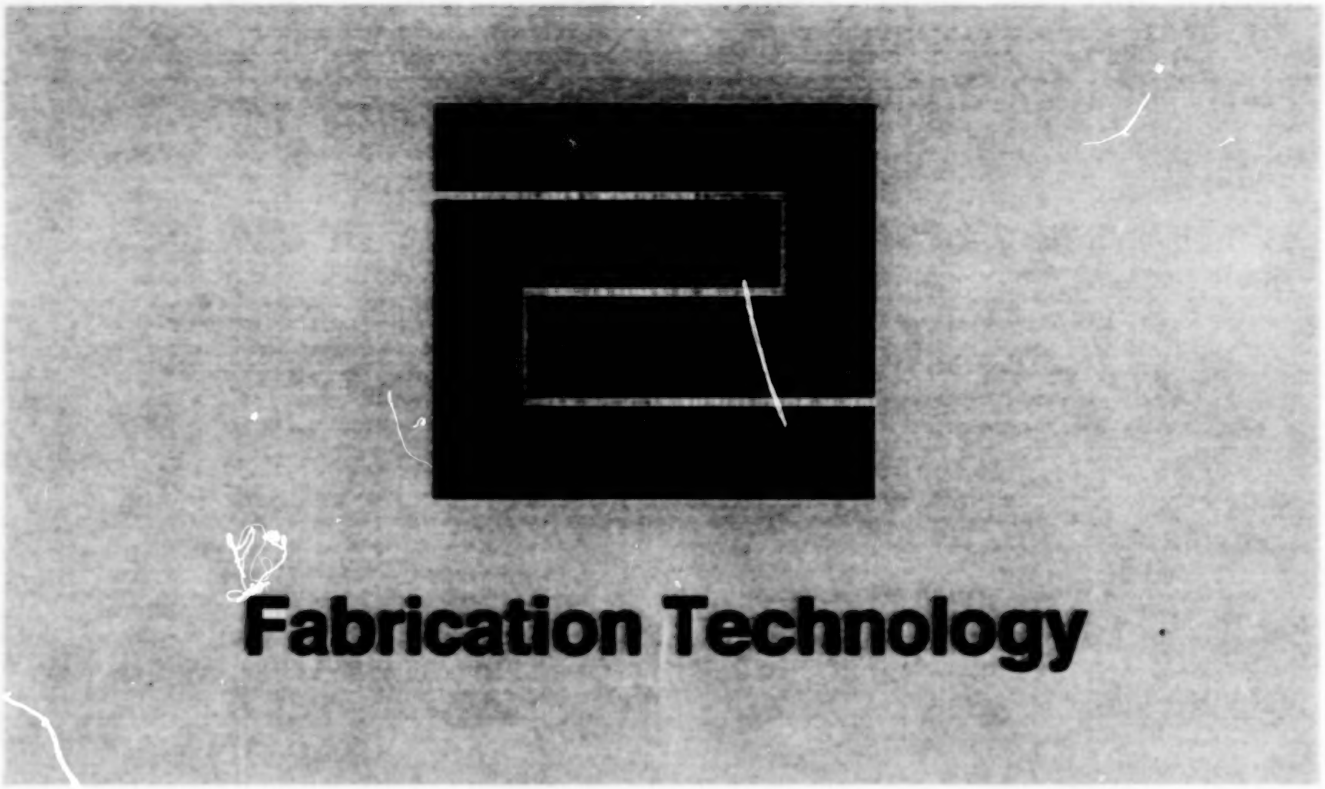

Fabrication Technology

Hardware, Techniques, and Processes

BLANK PAGE

Mounting Heater Wires on Glass Capillary-Heat-Transfer Tubes

The heaters performed flawlessly.

Lewis Research Center, Cleveland, Ohio

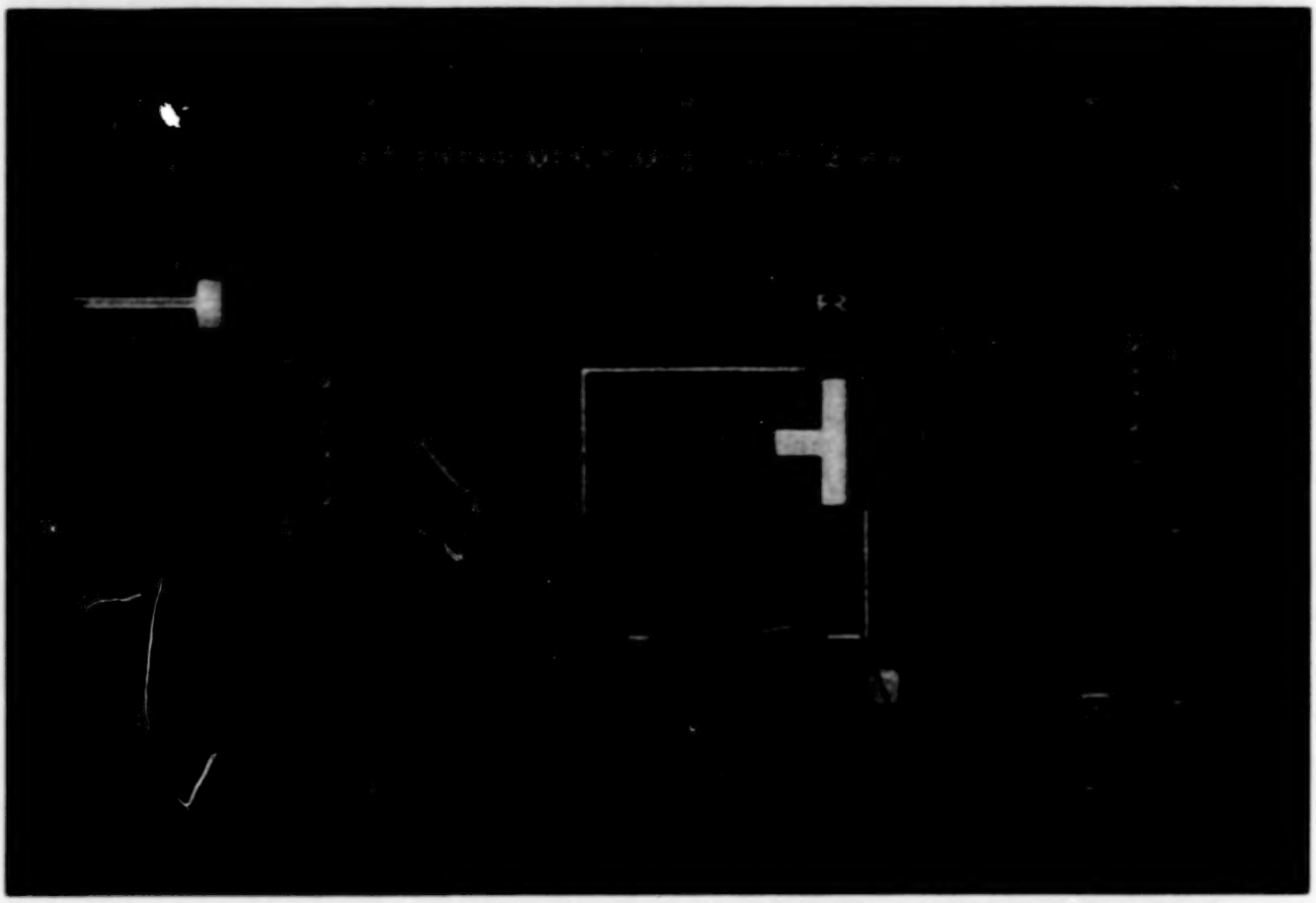

Heater Wires were mounted on adjacent cylindrical and conical portions of glass tubing used in a capillary-heat-transfer experiment.

Two mounting schemes were devised for attaching heater wires to special-purpose glass tubing used in a capillary-heat-transfer experiment. Not only were the wires required to supply heat needed for the experiment; in addition, it was required that the liquid and vapor enclosed by the tubing be visible between the wires. It was a challenge to satisfy these requirements while preventing (1) delamination of wires from the tubing and (2) short-circuiting that can occur as a consequence of delamination. Finally, neither the attachment nor the operation of the heaters could be allowed to impose stresses that could break the tubing.

The tubing was made from a low-thermal-expansion glass. The heater wires were made of a Cr/Co/Al/Fe alloy and had a diameter of 0.010 in. (0.25 mm). The problem was to mount one heater wire on a cylindrical section of capillary tube and the other wire on a conical transition between the capillary tube and wider evaporator/condenser tube (see figure).

Part of the solution to the wire-mounting problem was to prepare the capillary tube separately from the evaporator/condenser tube before bending the tubes and joining them to form the flow loop needed for the experiment. The main step in the separate preparation of the capillary tube was grinding a spiral groove, in which the heater wire would later be inserted. The spiral groove was intended to prevent adjacent turns of wire from sliding together and thereby becoming short-circuited. An additional advantage of placing the wire in the groove is that it increased the effective contact area between the wire and the tube, making for greater efficiency in the transfer of heat from the wire to the glass.

Once the groove was ground, the capillary and evaporator/condenser tubes were bent and then joined, with conical transition pieces, in a glass-blowing operation. A glass rod (not shown in the figure) was installed alongside the glass tubing to provide additional support for the capillary heater wire. The glass loop was stress-relieved. The capillary heater wire was inserted in the groove, then encapsulated in the groove by epoxy and a two-piece glass cover, which aided heat transfer while affording the required transparency.

The end portions of the heater wire were made to pass through two short ceramic tubes attached to the glass rod. The tips of the capillary heater wire were welded to copper wires, which were wider than the holes in the ceramic tubes; this arrangement prevented unwrapping of the capillary heater wire. The capillary-heater-wire installation stayed intact even when the heater was operated beyond the maximum use temperature of the epoxy.

Because the conical transition pieces were formed manually, they had irregular shapes, making it impractical to grind a spiral groove to hold a heater wire at the capillary/evaporator transition. Instead, all except the end portions of the wire for this location was bent in a serpentine configuration, then wrapped around the glass, then epoxied in place on the glass at each bend in the wire. The end portions of the wire were fed through a two-hole piece of ceramic and welded to larger wires; this arrangement prevented unwrapping and short-circuiting of the wire.

No failures of glass tubing were caused by the installation and operation of the heaters. Measurements by thermocouples confirmed that heat was transferred from the heater wires to the liquid in the glass. The heaters remained in contact with the glass, operating flawlessly throughout the capillary-heat-transfer experiment.

This work was done by Greg Blank of **Lewis Research Center**. *Further information is contained in a TSP [see page 1].*

Inquiries concerning rights for the commercial use of this invention should be addressed to NASA Lewis Research Center, Commercial Technology Office, Attn: Steve Fedor, Mail Stop 4–8, 21000 Brookpark Road, Cleveland, Ohio 44135. Refer to LEW-16707.

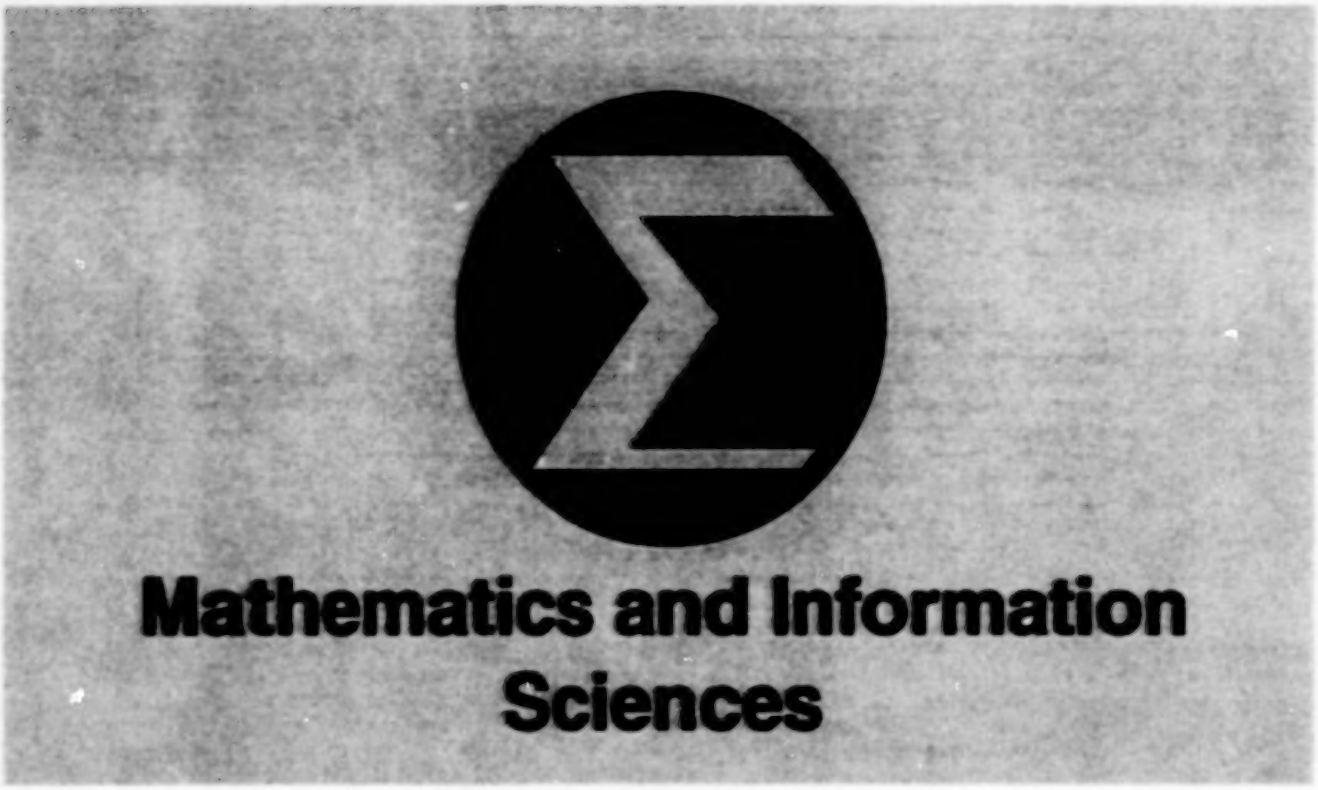

Mathematics and Information Sciences

Hardware, Techniques, and Processes

BLANK PAGE

ParVox — a Parallel-Processing Software for Volume Rendering of Data

Users could view results of simulations and modify underlying mathematical models "on the fly."

NASA's Jet Propulsion Laboratory, Pasadena, California

ParVox is a distributed visualization system consisting of a rendering core running on a parallel computer and a graphic user interface program (GUI) running on a Unix workstation. The ParVox system is designed for interactive, distributed visualization of large multiple time steps, multiple-parameter volume data sets: data sets that are impractical or impossible to visualize on workstations.

The following requirements were identified from discussion with scientists and are the basis for the design of ParVox:

1. Able to visualize a pregenerated volume data set interactively in three-dimensional (3-D) space or animate pregenerated multiple time-step volumes. Current visualizations include translucent colored volumes, isosurfaces representing threshold values, and 3-D slices of data.
2. Provide an application programming interface (API) for linking into applications. The API allows applications to render 4-D (spatial and time) volumes with predetermined parameters, such as classification, viewing transformation, shading, and lighting. Storing intermediate simulation results as rendered images greatly reduces the disk storage and the transmission time to the user's workstation.
3. Able to run in concert with the data generating application, all under the control of the GUI. This allows the researcher to view the model result while it is being generated and thus adjust the model parameters accordingly. This mode acts as both a visualization system and a debugging tool for the simulation by allowing analysis of results on the fly.

ParVox is designed to fulfill all of the above requirements. Currently, two of the three requirements have been implemented: It is able to visualize pregenerated data and has a full-featured rendering API.

As a post-processing distributed visualization system, it provides an X Window based GUI program for display and viewing control, a parallel input/output library for reading and writing 4-D volume data sets, a networking interface program that runs on parallel computer and calls the rendering API in response to the GUI workstation, and a parallel wavelet image-compression library that supports both lossless and lossy compressions.

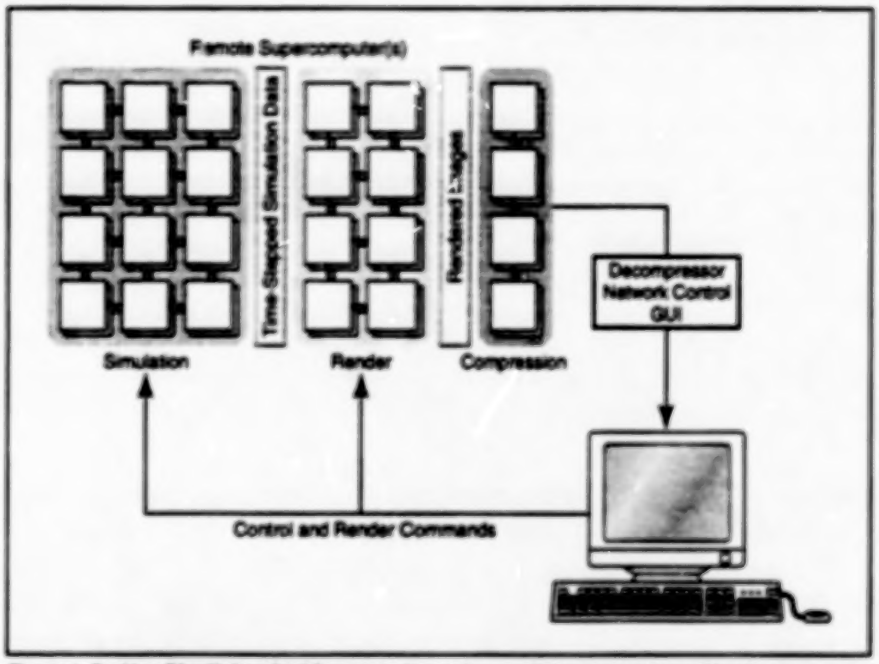

Figure 1. ParVox Pipelining Architecture allows the parallel computer to partition its resources optimally.

Figure 2. Atlantic Ocean Current Velocity Volume Data are shown with ocean floor topological map.

The ParVox rendering API is similar to OpenGL. It includes lighting, shading, classification, data redistribution, multiple isosurfaces, multiple slices, direct volume rendering, multiple variable and multiple time-step volume rendering. It uses the

"Splatting" algorithm, which is a feed-forward voxel projection algorithm.

A functional pipelining architecture is proposed to handle the third requirement (see Figure 1). This allows the parallel computer to partition its resources optimally for the simulation process and the rendering process separately.

The core ParVox is a scalable, efficient, parallel volume rendering API. Both object-space decomposition and image-space decomposition are used to assure balanced computational loads among parallel processors. An asynchronous, one-sided communication scheme is used for data transmission from splatting processors to compositing processors. The communication and synchronization overhead are minimized by overlapping the data transmission and computation.

ParVox is running on the Cray T3D and T3E supercomputers using Cray's shared memory (shmem) library. It is being ported to the Message Passing Interface Standard (MPI2.0); therefore, it will be portable to other supercomputer platforms. ParVox has been successfully used by JPL researchers in visualizing the Atlantic Ocean Current Simulation data (see Figure 2), the Thermal Convection Modeling data, and the BEAM (Beacon-based Exception Analysis for Multimissions) difference maps.

This work was done by P. Peggy Li and James Tsiao of Caltech and Scott Whitman of Equator Technology for **NASA's Jet Propulsion Laboratory**. *Further information is contained in a TSP [see page 1].*
NPO-20348

Improvements in Generating and Using Unstructured CFD Grids

A grid generation code accepts data directly from CAD software.

Lewis Research Center, Cleveland, Ohio

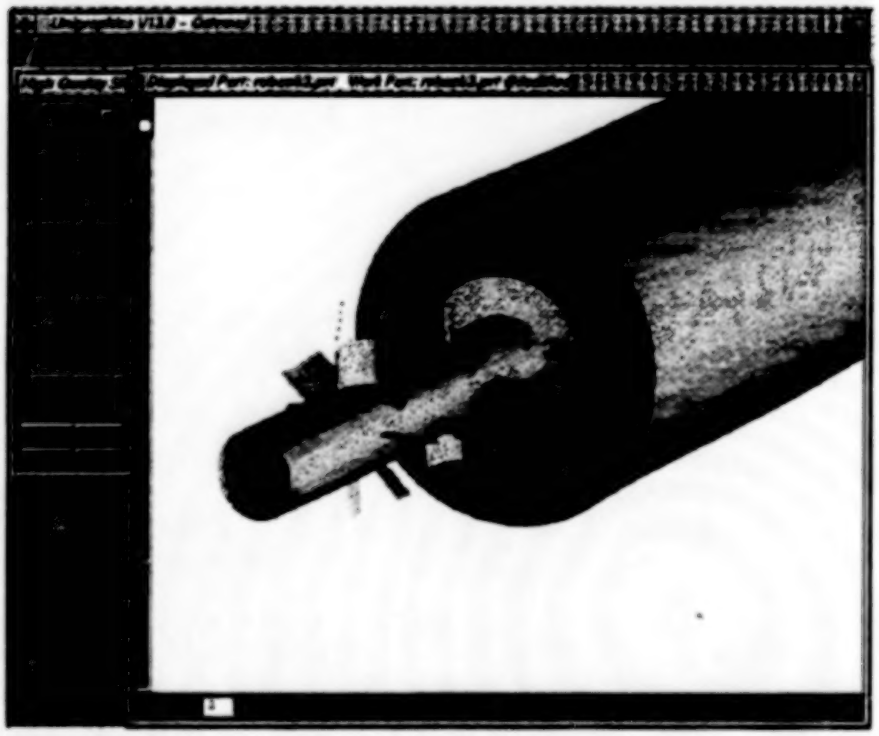

Figure 1. This is the original Unigraphics CAD Model of a vane configuration.

Some recent and continuing efforts to develop a software system for simulations of flows in gas-turbine combustors by Computational Fluid Dynamics (CFD) have addressed such major issues as the integration of CAD (Computer Aided Design) data for grid generation purposes. The generation of coordinate grids for use in flow-field computations is a major issue due to its time-consuming nature. The direct use and import of CAD data is important so as to remain true to the geometry and to reduce the user time necessary in generating the computational grid.

The software package CFD-GEOM, developed by CFD Research Corporation, has been modified to accelerate and optimize the generation of unstructured grids. [As used here, "unstructured" means having cells that are irregularly shaped and/or not necessarily connected in any particular sequence and are related to each other in arbitrary ways that must be specified explicitly.] The overall result was to provide within CFD-GEOM a fast and high-quality unstructured grid-generation capability. CFD-GEOM can generate grid combinations (i.e., hybrid grids) of tetrahedral, prismatic, and multiblock structured grids. The ability to generate those grids efficiently is of crucial importance to the NASA Lewis National Combustion Code, which supported some of those developments.

A critical factor in obtaining overall end-user efficiency is the access to the original CAD geometric description of the gas-turbine combustor. CFD-GEOM has incorporated several paths in which CAD data can be accessed and used. CFD-GEOM has implemented a robust IGES reader to enable the incorporation of CAD data stored in the IGES format. IGES is an international standard, enabling transfer of geometric CAD data between organizations if the CAD data base is not directly accessible. If the CAD data base is directly accessible, CFD-GEOM can obtain the geometric information from the data base without the need for IGES translation. This enables the grid-generation process access to the true CAD data without any inaccuracies which may occur through the IGES translation. Such a direct link also enables modifications made by the designer to be quickly received by the grid generator CFD-GEOM and incorporated into a CFD model.

CFD-GEOM, in collaboration with NASA Lewis, established a direct link with the Unigraphics CAD design system for transferring combustor design data directly to CFD-GEOM. This direct link allows combustor design engineers to access the data from Unigraphics directly in its true form. By accessing the data in this manner, CFD-GEOM is able to define surface sets, a collection of trimmed NURBS (Non-Uniform Rational B-Spline) surfaces which define a closed air-volume. The automatic definition of the surfaces which define this "air-vol-

ume" is crucial for the grid-generation process.

To prepare the geometric model for CFD (and other engineering) computations, a suitable grid must be generated to discretize the domain. For this purpose, CFD-GEOM has an automated (and controllable) unstructured grid-generation method which directly generates the grid on the trimmed NURBS model definition. The triangular surface mesh is generated on the NURBS surfaces using four constraints: maximum element size, transition factor (both are user specified), surface curvature criteria, and smallest geometric feature. The surface curvature criteria allows the user to specify how closely the surface needs to be approximated (i.e., more smaller elements in regions of high curvature). Once the initial surface mesh has been created, the user has the option to locally refine the surface grid as desired.

After a suitable triangular surface mesh is obtained, the volume grid-generation process can begin. Two options are available (1) generate a full tetrahedral mesh or (2) generate a prismatic grid by advancing the triangular cells into the normal direction of the surface over a certain user-specified distance and density. The latter option is usually combined with a tetrahedral mesh (i.e., hybrid volume grid) for the remainder of the computational domain. For the tetrahedral volume mesh generator, the user can control the grid density by using source parameters in the volumetric domain.

During the CFD-GEOM code-development process tremendous improvements have been made in speed and quality of the surface and volume mesher. A speed of 200,000 to 300,000 grid cells per minute is typical on high-end workstations, while grids with a minimal center-to-face angle of 15° can be reached for complex geometries. Both criteria are considered to be excellent values.

Figure 2. This is a CAD Model, directly imported from Unigraphics. It shows the tetrahedral grid generated by CFD-GEOM.

Using the procedure outlined, a significant reduction in time required to perform one gas-turbine combustor analysis cycle is evidenced. By directly accessing the data from the Unigraphics system (which is commonly used by some engine manufactures), the time required to do model set up has been minimized. With the use of fast and automatic grid-generation techniques, the time required for grid generation has been significantly reduced. In addition, high-quality grids tend to help the flow solver convergence process (fewer iterations on an iterative algorithm).

A demonstration of CFD-GEOM capabilities is given in Figure 1, which shows the original CAD model of a vane configuration within the Unigraphics CAD system (CAD model courtesy of Pratt & Whitney). Figure 2 depicts the resulting surface mesh and a slice of the tetrahedral field grid.

This work was done by John Whitmire, Tim Dollar, Vincent Harrand, and Curtis Mitchell of CFD Research Corporation for NASA **Lewis Research Center**. *Further information is contained in a TSP [see page 1].*

Inquiries concerning rights for the commercial use of this invention should be addressed to NASA Lewis Research Center, Commercial Technology Office, Attn: Steve Fedor, Mail Stop 4–8, 21000 Brookpark Road, Cleveland, Ohio 44135. Refer to LEW-16583.

Using Genetic Algorithms in Spacecraft Vibration Control

Three developmental computer programs would provide for robust, reconfigurable, high-performance control.

American GNC Corporation, Chatsworth, CA

Three software products are being developed to help satisfy the needs of NASA and of private industry for reconfigurable active control systems to suppress vibrations in Reusable Launch Vehicles (RLVs) and other structures. These potentially highly marketable products are the following:

- The Integrated Structural Modeling and Intelligent Control Toolbox serves as a software environment for mathematical modeling, analysis, design, simulation, and implementation of genetic-algorithm-based "intelligent" control of vibrations in structures.
- The Intelligent Distributed Structural Control Node is a real-time software prototype of a distributed control system that employs distributed fuzzy-logic structural controllers and a fuzzy neural reconfiguration strategy.
- The Distributed Health Monitoring and Decision-Making Integration System is a software system for genetic-algorithm-based, decentralized, parallelized fault detection and isolation (FDI) and reconfiguration.

The need for these products arises from the following considerations: Active control for suppressing vibrations in spacecraft is a

topic of considerable importance, especially lately, given the advent of Reusable Launch Vehicles (RLVs). One of the difficulties in designing capable controllers for space structures lies in the inability to obtain or to test accurate mathematical models of their dynamics, including submodels of vibration modes, prior to launching the structures into outer space. Thus, in designing a vibration controller for a space structure, it becomes a requirement to provide robustness against all possible uncertainties. Ideally, the structure vibration controller should be able to both characterize the dynamics of the structure and modify its dynamical model after launch, thereby affording both superior robustness and excellent performance.

Also, the stability of individual components on RLVs is an issue of grave concern. Stiffening these components often entails adding undesirable weight. The characterization of these components and the attenuation of their accelerations, by use of a "smart" active vibration-control system, are of the utmost importance in an effort to attain the all-consuming goal of minimizing RLV weight.

Other important issues related directly to the vibration-control issue include the need to protect expensive, fragile payloads, to release them into their orbits as accurately as possible. An accurate and efficient placement and/or pointing of a payload to be released into orbit from an RLV an application of enormous commercial value.

The three software products mentioned above take advantage of active vibration control methods and equipment, including "smart" piezoelectric sensors, actuators, and sensor/actuator units. Genetic algorithms serve as means for optimization and learning. These three products implement genetic-algorithm-based techniques of "intelligent," reconfigurable active vibration control developed by American GNC Corp.

Potential applications for the three software products include attenuation of accelerations for space-based experimentation in combustion and growth of crystals, enhancing spacecraft and aircraft ride qualities, extending the lives of aircraft and spacecraft by minimizing the damage wrought by structural vehicle vibrations, and extending the lives of airplanes by minimizing loads on wing roots. Also, these products and the associated techniques can be used for high-precision pointing and active control of vibrations of civilian and military flexible structural systems, including optomechanical systems, aerospace structures, weapon systems, positioning machines, and robotics.

This work has been and will be undertaken by the **American GNC Corporation**, *9131 Mason Avenue, Chatsworth, CA 91311, an SBA 8(a) certified Small Disadvantaged Business concern, as part of a NASA Small Business Innovative Research (SBIR) project monitored by* **Marshall Space Flight Center**. *The NASA SBIR Contract Number is NAS8-98101; Topic: 97-1 08.01; Topic Title: Launch Vehicle Technologies. For further information, contact Dr. Ching-Fang Lin, American GNC Corporation, at tel: (818) 407-0092, fax: (818) 407-0093, or e-mail: cflin@americangnc.com.*
SBIR0006

Recursive and Adjacency Algorithms for Ranking Hypotheses

A library of computer programs has been developed to solve the problem of parametric ranking of a set of hypotheses on the basis of incomplete and/or uncertain information. In general, the ranking must be learned by use of training examples in which one observes the values of random variables that depend on the hypotheses and adjusts the parameters accordingly. In addition, it is necessary to balance a potential increase in confidence in the ranking against the cost of additional examples. In these programs, the balance is struck by use of a combination of the "probably approximately correct" criterion from the theory of computational learning and the "expected loss" criterion from decision theory and gaming problems. The library offers the option to use a ranking algorithm that performs a recursive selection among the remaining unranked hypotheses, and/or one that performs only pairwise comparisons between adjacent hypotheses. These programs are written in ANSI C++. In tests on data from real-world problems, including scheduling and spacecraft design, these programs outperformed older hypothesis-ranking software.

This program was written by Steve A. Chien, Andre Stechert, and Darren Mutz of Caltech for **NASA's Jet Propulsion Laboratory**. *Further information is contained in a TSP [see page 1].*
NPO-20170

National Aeronautics and
Space Administration

END

04\23\99